Journal of Molecular Histology (2025) 56:106
https://doi.org/10.1007/s10735-025-10382-x

ORIGINAL PAPER

Exogenous mitochondria added on benefits for cellular prion protein overexpression in adipose-derived mesenchymal stem cells treatment on intracranial hemorrhage rat

Kun-Chen Lin[1] · Jui-Ning Yeh[2,3] · Pei-Hsun Sung[4,5,6] · Tsung-Cheng Yin[7,8] · John Y. Chiang[9,10] · Chi-Ruei Huang[4,5] · Yi-Ling Chen[4,6] · Yi-Ting Wang[4,6] · Kuan-Hung Chen[1] · Hon-Kan Yip[4,5,6,11,12]

Received: 8 October 2024 / Accepted: 21 February 2025 / Published online: 13 March 2025

Abstract

We examined whether combined exogenous mitochondria (Ex^{Mito}) and cellular prion protein overexpression (Ove-PrP^{C}) in adipose-derived mesenchymal stem cell (Ove-PrP^{C} in ADMSCs) therapy is superior to a single therapy for protecting the brain against intracranial hemorrhage (ICH) in rats. In vitro, compared with the control group, Ex^{Mito} transfusion into recipient cells (i.e., N2a cells) significantly increased under hypoxic conditions ($P<0.001$) and augmented ρ0 cell proliferation and cell-cycle activation ($P<0.001$). PrP^{C-OE} in ADMSCs exhibited higher resistance to H_2O_2-induced cell senescence and mitochondrial and DNA damage compared to ADMSCs ($P<0.001$). Rats were categorized into group 1 (sham-control), 2 (ICH), 3 [ICH + Ex^{Mito} (350 μg) by intracranial injection at 3 h after ICH], 4 [ICH + PrP^{C-OE} in ADMSCs (6.0×10^5 cells) and intracranial injection and 1.2×10^6 cells by intravenous injection)], and 5 (ICH + combined Ex^{Mito} + PrP^{C-OE} in ADMSCs). By day 28, the brain infarct volume, brain infarct area, inflammatory cell infiltration, and biomarkers for DNA and mitochondrial damage were highest in group 2, lowest in group 1, and significantly lower in group 5 than in groups 3 and 4. NeuN cells exhibited the opposite pattern for brain infarct volume, and neurological function (corner test) significantly improved in groups 3 and 4, with further improvement in group 5 compared with that in group 2 ($P<0.0001$). Combined Ex^{Mito} + PrP^{C-OE} ADMSCs therapy was superior to either therapy alone in mitigating the ICH-induced brain damage.

Keywords Intracranial hemorrhage · Mitochondria · Cellular prior protein overexpression · Adipose derived mesenchymal stem cells

Introduction

Stroke is a leading cause of death and permanent neurological sequelae worldwide (Collaborators 2019; Kim et al. 2020; Padovani and Pilotto 2020). It is categorized as ischemic stroke (IS) or hemorrhagic stroke (HS) (Bamford et al. 1991; Chen et al. 2014a; An et al. 2017; Ojaghihaghighi et al. 2017). HS is further divided into intracerebral hemorrhage (ICH) and subarachnoid hemorrhage, typically resulting from arterial rupture (Bamford et al. 1991; Chen et al. 2014a; An et al. 2017; Ojaghihaghighi et al. 2017). Although HS accounts for less than 30% of strokes (Bamford et al. 1991; Chen et al. 2014a; An et al. 2017; Ojaghihaghighi et al. 2017), it is associated with higher mortality and a greater risk of permanent neurological sequelae compared to IS (Montano et al. 2021; O'Carroll et al. 2021; Unnithan and Mehta 2023). IS treatment has advanced considerably in recent years with promising outcomes (StatPearls Publishing et al. 2023; Minnerup et al. 2016; Rangel-Castilla et al. 2016; Rodrigues et al. 2016; Henderson et al. 2018; Powers et al. 2018, 2019; Smith 2019; Albay et al. 2020; Xiong and Bath 2020), but the treatment of HS, particularly in ICH, has remained largely unchanged for decades (Gauberti et al. 2021; Hemphill et al. 2015; Hostettler et al. 2019). Standard interventions for ICH, including surgical procedure and intensive medical management, are commonly utilized for

Extended author information available on the last page of the article

patients with ICH, resulting in a high incidence of mortality and disability, often severely limiting patients' employability and social engagement (Reyes et al. 2019; Mittal and Lele 2011; Pinzon and Wijaya 2020). Therefore, developing a safe and effective new treatment modality and ICH is of paramount importance.

In ICH, loss of blood supply and increased pressure due to hematoma/brain edema lead to oxidative stress, inflammatory reactions, nutrient deprivation, and the coagulation response, which, in turn, causes ischemia-related and oxidative stress-induced mitochondrial damage and eventually exhausts ATP-derived energy (Haupenthal et al. 2021; Testai and Aiyagari 2008; Gaiqing 2014; Duan et al. 2016; Hu et al. 2016; Mittal and LacKamp 2016; Zheng et al. 2016; Burchell et al. 2017; Shao et al. 2019). Together, these factors create a vicious cycle and toxic environment (Testai and Aiyagari 2008; Gaiqing 2014; Duan et al. 2016; Burchell et al. 2017; Shao et al. 2019) that is unfavorable for the survival of neurons and brain tissue, resulting in severe brain architectural damage, neurological dysfunction, and high mortality.

We previously demonstrated that exogenous mitochondria can be transferred into recipient cells (Wu et al. 2021; Lee et al. 2018; Lin et al. 2018; Yip et al. 2020) and that cell–cell mitochondrial transfer occurs (Yip et al. 2020). Furthermore, we showed that exogenous mitochondrial transfer can improve neurological outcomes in rodents after acute IS (Yip et al. 2020). Our recent studies revealed that intravenous administration of exogenous mitochondria salvaged the lung from acute respiratory distress syndrome (Lee et al. 2018; Yip et al. 2020). Considerably, we demonstrated that adipose-derived mesenchymal stem cell (ADMSCs) therapy improves organ dysfunction caused by different disease entities (Yip et al. 2021a, 2013; Weissmann 2004; Chen et al. 2014b, 2016a; Lin et al. 2016; Ko et al. 2020), mainly through anti-inflammation, immunomodulation, and neurogenic regeneration (Weissmann 2004; Chen et al. 2014b; Lin et al. 2016; Ko et al. 2020).

The cellular prion protein (PrP^C) was first identified as a glycosylphosphatidylinositol-anchored glycoprotein that is mainly expressed in the neurological system (i.e., brain and nerve cells) and other tissues (Yip et al. 2021a; Lin et al. 2020). Later, PrP^C serving as a neuroprotective or neurosurvival protein was shown to prevent Bcl-2-linked protein X (Bax)-mediated cell death (Zomosa-Signoret et al. 2008). Our recent in vitro study demonstrated that overexpression of cellular prion protein (Ove-PrP^C) in ADMSCs resulted in a strong capacity to resist oxidative stress and upregulate cell viability and the cell proliferation rate. Additionally, Ove-PrP^C in ADMSCs protected the rodent kidney against ischemia–reperfusion injury by enhancing ATP and mitochondrial biogenesis, which subsequently downregulated oxidative stress (Roucou et al. 2005). Based on these studies, combined therapeutic approach with exogenous mitochondria and Ove-PrP^C in ADMSCs may surpass the efficacy of either intervention alone in protecting neurological function and the brain architecture in the context of acute ICH-induced injury in rat model.

Results

Exogenous mitochondria ($Ex.^{Mito}$) in recipient cells, oxygen consumption rate (OCR), and hypoxia-triggered changes in mitochondrial bioenergetics (Fig. 1)

Real-time qPCR was performed to determine the mitochondrial DNA copy number. The results demonstrated that the relative mitochondria DNA copy number was significantly higher in the Neuro-2a cells (N2a) cells + Ex^{Mito} and N2a cells + hypoxia + Ex^{Mito} groups than in the N2a cells only and N2a cells + hypoxia groups (Fig. 1A). Ex^{Mito} (i.e., donor) was transferred into N2a cells (i.e., recipient), particularly under hypoxic conditions, indicating that these cells can take up Ex^{Mito} for energy utilization and survival.

Additionally, to estimate the efficiency and regulation of mitochondrial respiration, groups A1 (N2a), A2 (N2a cells + exogenous mitochondria)], A3 (N2a cells + $CoCl_2$) and A4 (N2a + $CoCl_2$ + Ex^{Mito}) were evaluated using Seahorse XF24 extracellular flux analysis, which measures the OCR (Fig. 1B). The results showed that the OCR was remarkably high, indicating high mitochondrial respiration and that exogenous mitochondrial function was preserved during isolation and at the time of transfer (Fig. 1B). Additionally, parameters of mitochondrial respiration (Fig. 1C–F), including basal respiration (Fig. 1C), ATP production (Fig. 1D), maximal respiration (Fig. 1E), spare respiratory capacity (Fig. 1F), and proton leakage (Fig. 1G), were lowest in A3, highest in A4, and notably higher in A2 than in A1.

$Ex.^{Mito}$ was recognized and transferred into N2a cells (Fig. 2)

To verify whether Ex^{Mito} could be transferred into N2a cells (i.e., recipient cells), N2a cells were categorized into the four groups described in Fig. 1 (from A1 to A4). The immunofluorescence (IF) microscopy findings of endogenous and Ex^{Mito} staining using MitoTracker (Fig. 2A–L) demonstrated that endogenous mitochondria (Fig. 2M) were significantly lower in A3 and A4 than in A1 and A2, whereas Ex^{Mito} (Fig. 2N) was significantly increased in A2, and more significantly increased in A4 than in A1 and A3. The

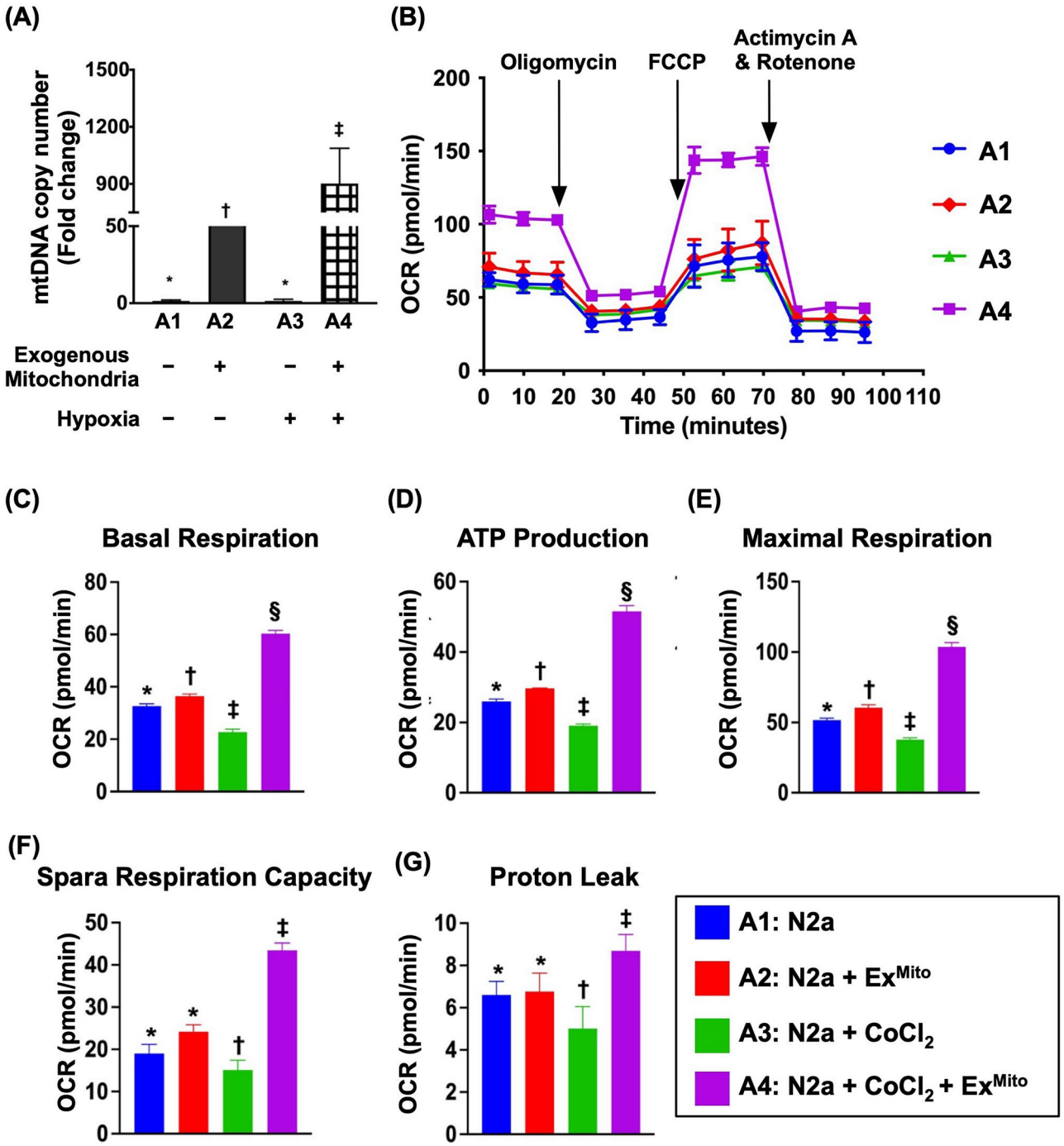

Fig. 1 Exogenous mitochondria (Ex^{Mito}) in recipient cells, OCR and hypoxia-triggered changes in mitochondrial bioenergetics. (A) Real time qPCR for quantification of mitochondrial DNA copy number was conducted and the result showed that relative mitochondria DNA expression was significantly higher in N2a cells + exogenous mitochondria and more significantly higher in N2a cells + hypoxia + mitochondria, * vs. other groups with different symbols (†, ‡), $P < 0.0001$ (n = 4 for each group). (B) Time courses of mitochondrial respiration of N2a cells after different strategic treatments. Mitochondrial respiration reflected by the level of oxygen consumption rate (OCR) in four groups (n = 4 per group), followed by injection of oligomycin, FCCP and antimycin A/rotenone. The result showed highly efficacious mitochondrial respiration rate. (C–G) Showing the statistical analyses for the rates of basal respiration (C), ATP production (D), maximal respiration (E), spare respiratory capacity (F) and proton leak (G). Analytical results of (C), (D), (E) and (F), * vs. other groups with different symbols (†, ‡, §), $P < 0.0001$. On the other hand, analytical result of (G), * vs. other groups with different symbols (†, ‡), $P < 0.001$. (n = 4 per group). All statistical analyses were performed by one-way ANOVA, followed by Bonferroni multiple comparison post hoc test (n = 4 for each group). Symbols (*, †, ‡, §) indicate significance (at 0.05 level). OCR = oxygen consumption rate; mt = mitochondria. A1 = N2a, A2 = N2a cells + exogenous mitochondria (Ex^{Mito}), A3 = N2a cells + $CoCl_2$, A4 = N2a + $CoCl_2$ + Ex^{Mito}

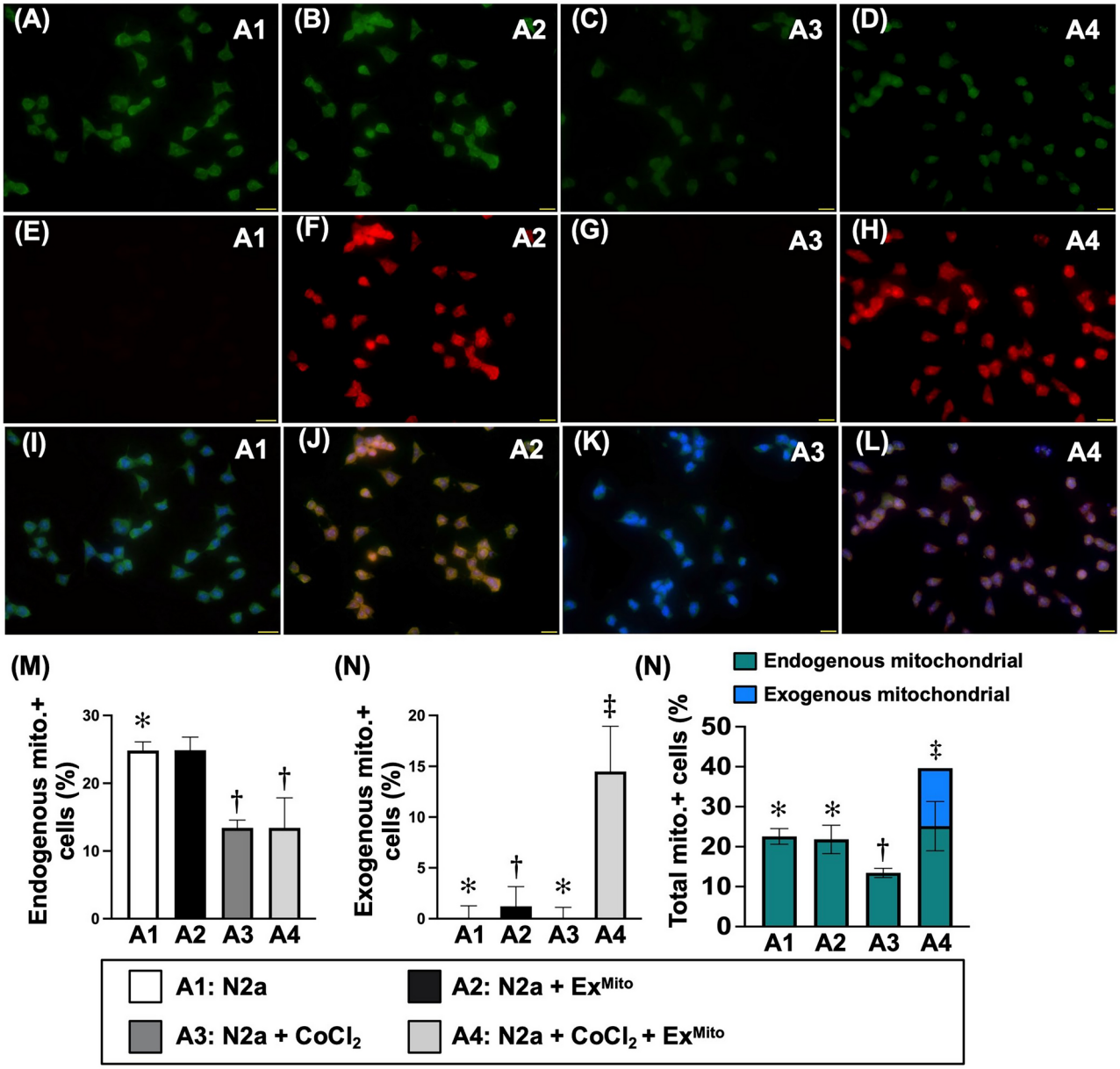

Fig. 2 Ex^{Mito} were recognized to be transferred into N2a cells. (A–L) Illustrating the immunofluorescent (IF) microscopic finding (400x) for identification of endogenous (A–D) (green color), exogenous (E–H) (red color) and merged (I–L) (pink-color) (noted that blue color was DAPI stain for identification of nuclei) mitochondrial staining by Mito-tracker. (M) Analytical result of endogenous mitochondrial expression, * vs. †, $P<0.001$. (N) Analytical result of exogenous mitochondria, * vs. other groups with different symbols (†, ‡), $P<0.001$. * vs. other groups with different symbols (†, ‡), $P<0.001$. (O) Analytical result of total mitochondrial expression in N2a cells, * vs. other groups with different symbols (†, ‡, §), $P<0.0001$. vs. other groups with different symbols (†, ‡, §), $P<0.0001$. All statistical analyses were performed by one-way ANOVA, followed by Bonferroni multiple comparison post hoc test (n = 4 for each group). Symbols (*, †, ‡, §) indicate significance (at 0.05 level). A1 = N2a, A2 = N2a cells + Ex^{Mito}, A3 = N2a cells + $CoCl_2$, A4 = N2a + $CoCl_2$ + Ex^{Mito}

total mitochondrial content (Fig. 2N) was notably higher in group A4 than in the other groups.

ADMSCs-derived mitochondria were transferred into ρ0 cells through tunneling nanotubes (TNT) (Fig. 3)

Next, to confirm that ADMSCs-derived mitochondria could be transferred into ρ0 cells (mitochondrial-DNA depleted cells) through the TNT system, in vitro analysis was performed using IF microscopy. Few mitochondria were identified in ρ0 cells (Fig. 3A–E), suggesting that mitochondria were depleted from N2a cells. Additionally, the TNT system transferred positively MitoTracker-stained mitochondria from ADMSCs to ρ0 cells (Fig. 3F–J), suggesting that mitochondria can donated to recipients through cell-to-cell interactions and the TNT delivery system.

$Ex.^{Mito}$ treatment augmented N2a cell proliferation (Fig. 4)

To determine whether exogenous mitochondrial treatment enhances N2a cell proliferation during cell culture, IF microscopy was utilized in vitro. The cellular expression of Ki67 + (Fig. 4A–G) and PCNA + (Fig. 4H–N) cells, two indicators of cell proliferation, was significantly lower in hypoxia-treated N2a cells and ρ0 cells but was significantly reversed after Ex^{Mito} addition.

Impact of Ove-PrP^C in ADMSCs on ameliorating oxidative stress-induced cell senescence, DNA and mitochondrial damage, and augmenting the cell cyclins and cell proliferation at molecular-cellular levels (Figs. 5, 6)

To examine whether Ove-PrP^C in ADMSCs reduced cell senescence and DNA and mitochondrial damage, ADMSCs were categorized as C1 (ADMSCs), C2 (Ove-PrP^C in ADMSCs), C3 (ADMSCs + H_2O_2), and C4 (Ove-PrP^C in ADMSCs + H_2O_2). The result showed that cellular expressions of

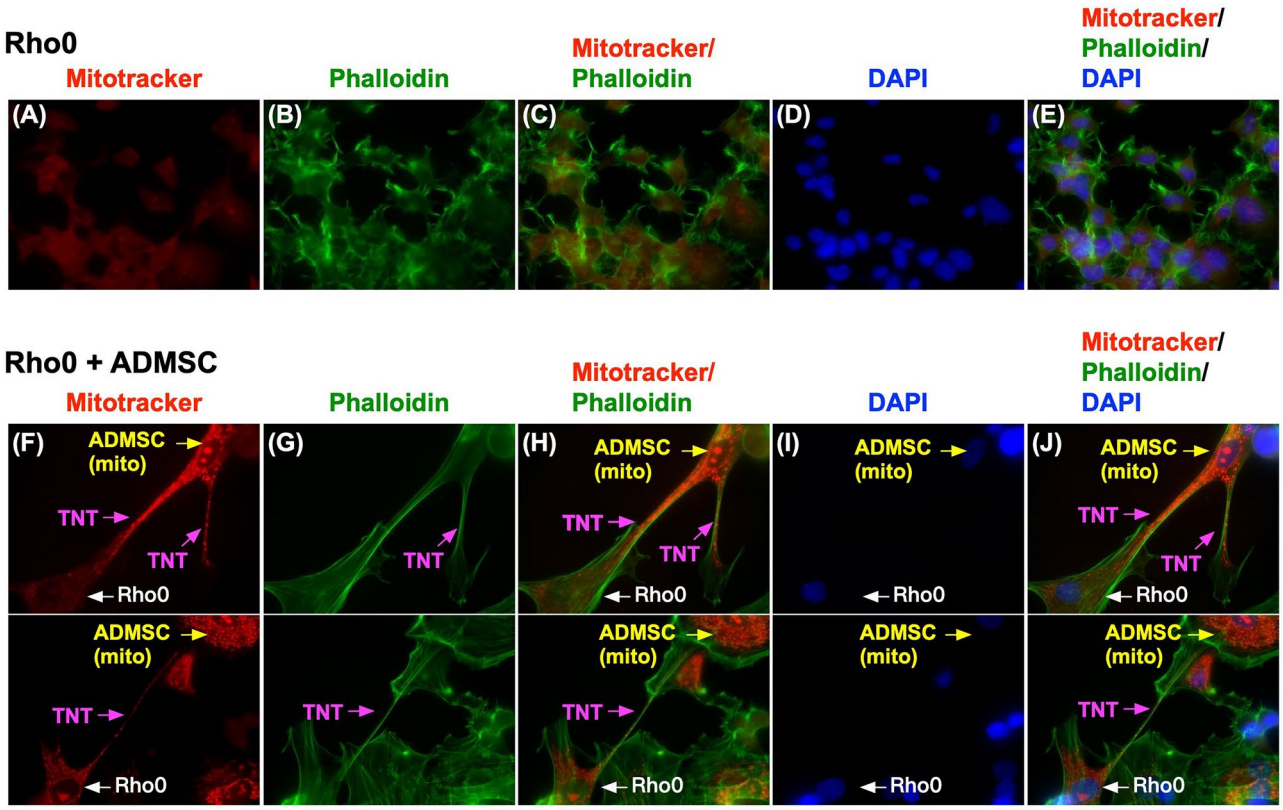

Fig. 3 ADMSCs-derived mitochondria could be transferred into the ρ0 cells through tunneling nanotubes (TNT). (A–E) Illustrating the immunofluorescent (IF) microscopic finding (400x) for identification of the endogenous mitochondria in ρ0 cells (i.e., ρ0 cells were the mitochondrial-DNA depleted cells). The result demonstrated that only a rare number of mitochondria was identified in the ρ0 cells (red color in A). (F–I) Illustrating the ADMSCs mitochondrial staining (red color. i.e., Mitotracker stain) and cytoskeleton (green color, i.e., phalloidin stain). The result showed that the TNT (pink arrows) transferred the positively Mitotracker stained mitochondria to ρ0 cells (white arrows) which were clearly identified. Yellow arrows indicated ADMSCs mitochondria. Scale bar in right lower corner represents 20 µm

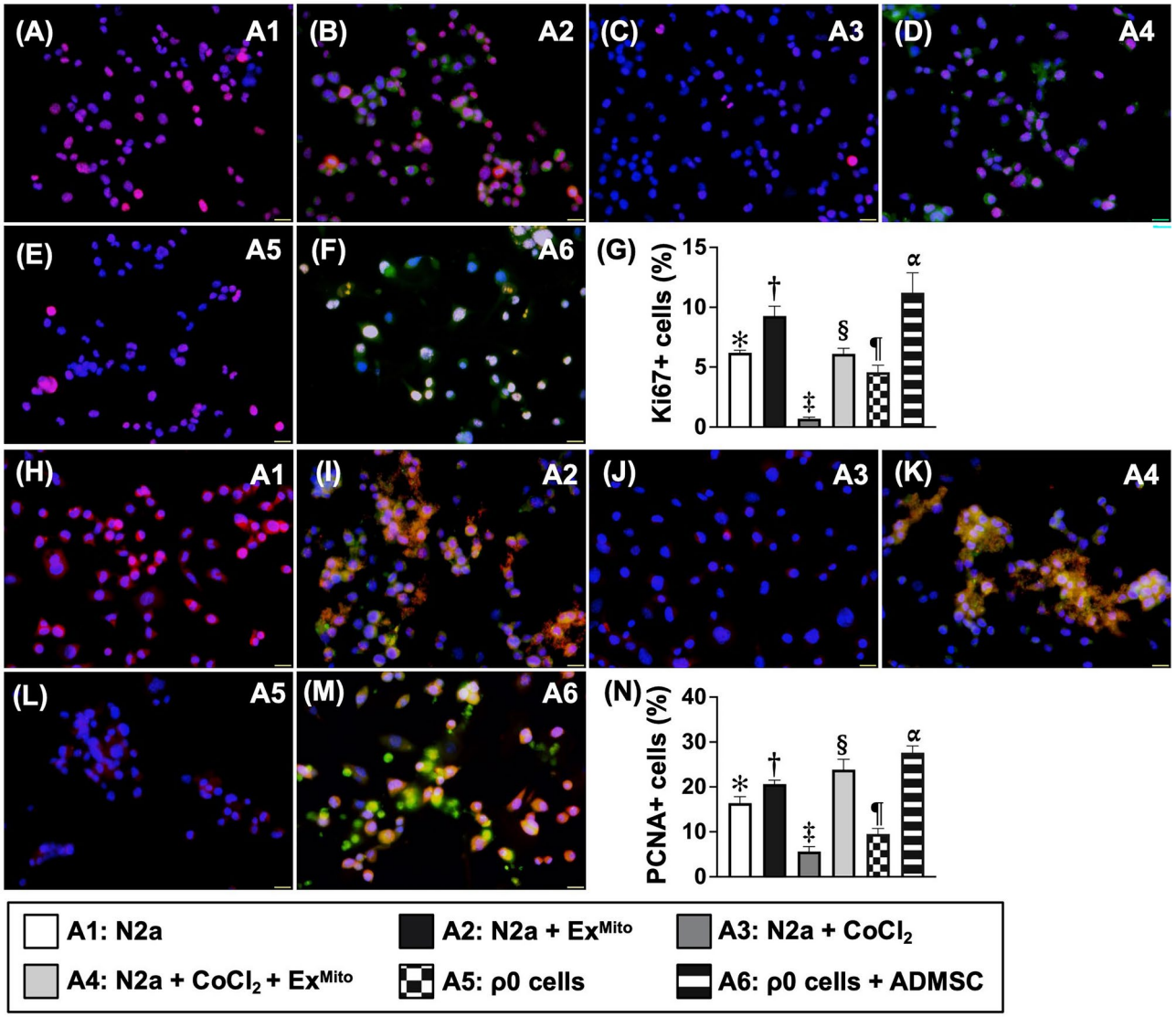

Fig. 4 Ex^{Mito} treatment augmented N2a cell proliferation. (A–F) Illustrating the IF microscopic finding (400x) of merged picture [i.e., including Ki67 stain (red color) and mitochondrial stain (green) color] for identification of Ki67+cells (pink color). Blue color indicated DAPI satin for identification of nuclei. (G) Analytical result of number of Ki67+cells, * vs. other groups with different symbols (†, ‡, §, ¶, α), $P<0.0001$. (H–M) Illustrating the IF microscopic finding (400x) of merged picture [i.e., including PCNA stain (red color) and mitochondrial stain (green) color] for identification of PCNA+cells (pink color). Blue color indicated DAPI satin for identification of nuclei. (N) Analytical result of number of PCNA+cells, * vs. other groups with different symbols (†, ‡, §, ¶, α), $P<0.0001$. Scale bar in right lower corner represents 20 µm. All statistical analyses were performed by one-way ANOVA, followed by Bonferroni multiple comparison post hoc test (n=6 for each group). Symbols (*, †, ‡, §, α) indicate significance (at 0.05 level). A1=N2a, A2=N2a cells+Ex^{Mito}, A3=N2a cells+$CoCl_2$, A4=N2a+$CoCl_2$+Ex^{Mito}, A5=ρ0 cells, A6=ρ0 cells+ADMSCs

β-galactosidase (Fig. 5A–E), an index of cell senescence, and γ-H2AX (Fig. 5F–J), an indicator of DNA damage, were significantly higher in C3 than in C1 and C2 but significantly reversed in C4; there was no difference between C1 and C2. Mitochondrial cytochrome C (Fig. 5K–O), an indicator of mitochondrial integrity, showed the opposite pattern as γ-H2AX among the groups. Our findings indicate that Ove-PrP^C in ADMSCs attenuated the damage caused by H_2O_2 (i.e., oxidative stress) in cells.

Western blot analysis revealed that the protein levels of PrP^C (Fig. 6A) and Ki67 (Fig. 6B) (cell proliferation markers) were significantly higher in C2 than in C1. Additionally, the protein expressions of NOX1 (Fig. 6C) and NOX-4 (Fig. 6D), two indices of oxidative stress; protein expressions of cyclophilin D (Fig. 6E) and p-DRP1 (Fig. 6F), two indicators of mitochondrial damage; and protein expressions of cleaved caspase 3 (Fig. 6G), cleaved PARP (Fig. 6H) and Bax (Fig. 6I), three indices of apoptosis, were the highest in C3, lowest in C2, and significantly higher in C4 than in C1.

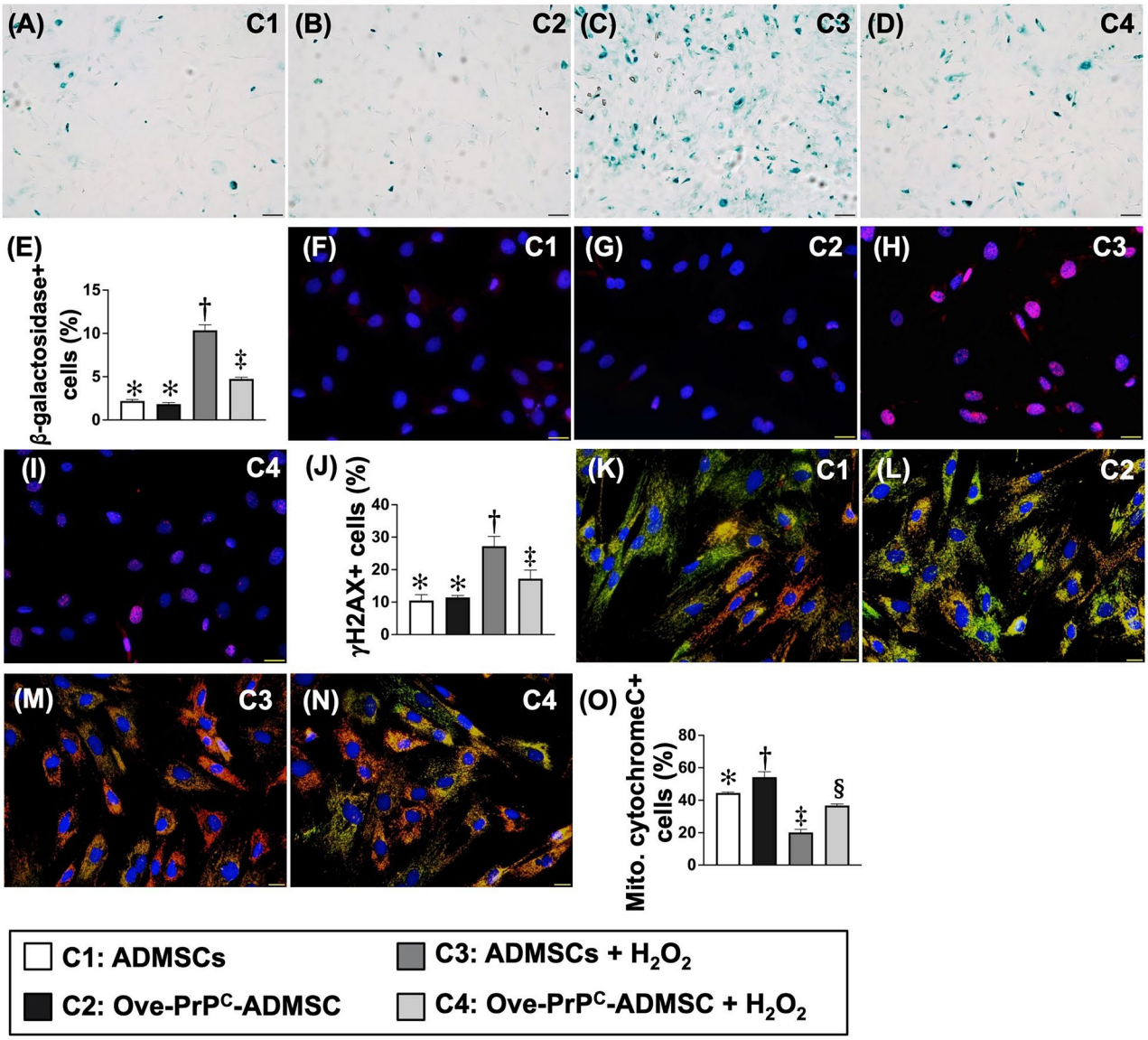

Fig. 5 Ove-PrP^C in ADMSCs alleviated the oxidative stress-induced cellular levels of senescence, DNA damage and impairment of mitochondrial functional integrity. (A–D) Illustrating the immunohistochemical staining (100x) for identifying the expression of ADMSCs senescence indifferent condition (blue-green color). Scale bar in right lower corner represents100 µm. (E) Analytical result of number of β-galactosidase+cells, * vs. other groups with different symbols (†, ‡), $P<0.0001$. (F—I) Illustrating the IF microscopic finding (400x) for identification of cellular expression of γ-H2AX (pink color). Scale bar in right lower corner represents 20 µm. (J) Analytical result of number of γ-H2AX+cells, * vs. other groups with different symbols (†, ‡), $P<0.0001$. (K–N) Illustrating the IF microscopic finding (400x) for identification of the expression of mitochondrial cytochrome C (green-purpose color indicated a merge picture by double stains of cytochrome C [(green color) and HSP60 (red color)]. Scale bar in right lower corner represents 20 µm. (O) Analytical result of number of mitochondrial cytochrome C+cells, * vs. other groups with different symbols (†, ‡, §), $P<0.0001$. All statistical analyses were performed by one-way ANOVA, followed by Bonferroni multiple comparison post hoc test (n=4 for each group). Symbols (*, †, ‡) indicate significance (at 0.05 level). ADMSCs=adipose-derived mesenchymal stem cells; Ove-PrP^C=overexpression of cellular prion protein. C1=ADMSCs, C2=Ove-PrP^C in ADMSCs, C3=ADMSCs+H_2O_2, C4=Ove-PrP^C in ADMSCs+H_2O_2

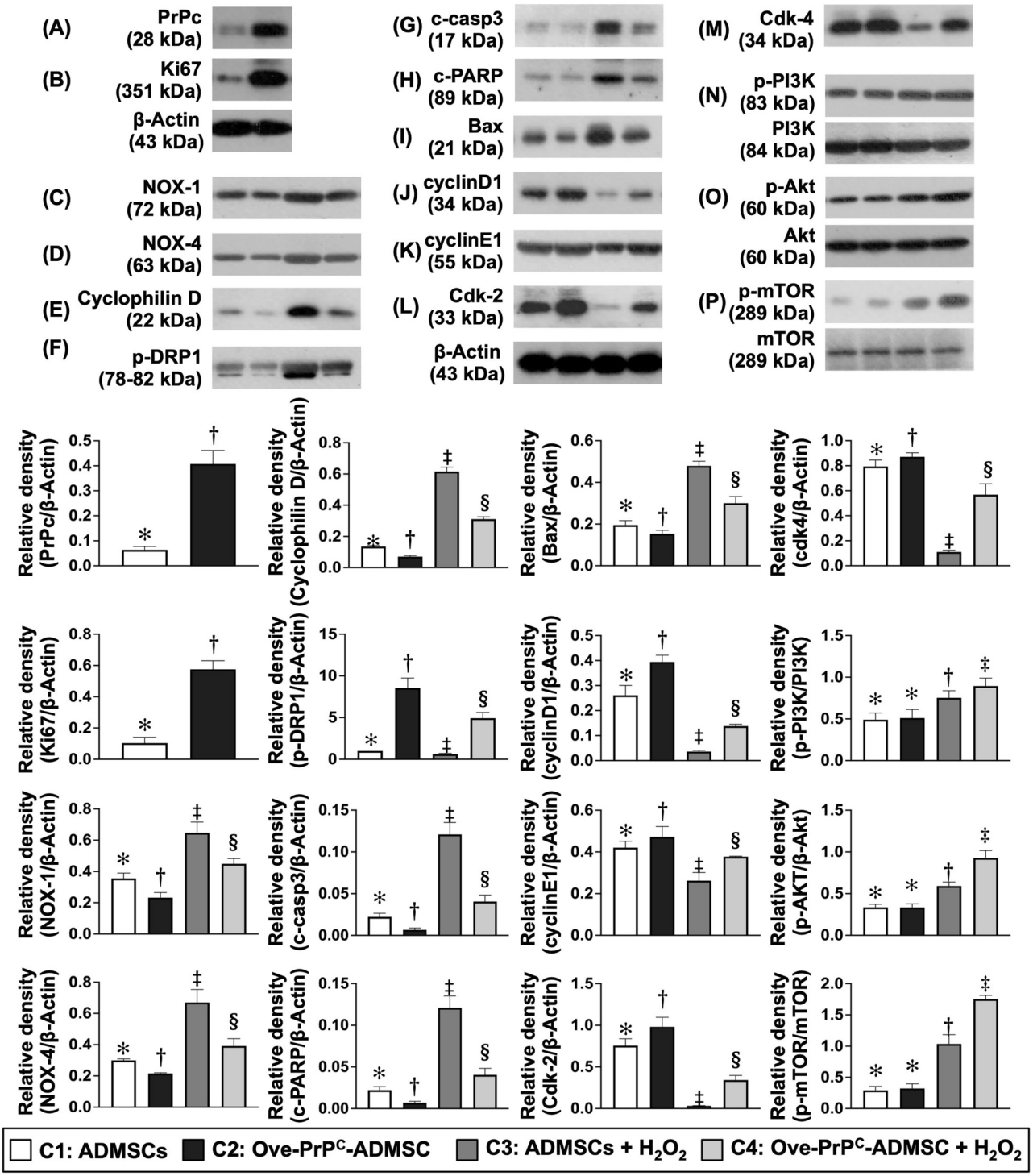

In contrast, the protein levels of cyclin D1 (Fig. 6J), cyclin E1 (Fig. 6K), cdk-2 (Fig. 6L) and cdk-4 (Fig. 6M), four indicators of cell cyclins, displayed an opposite pattern of oxidative stress among the groups. Additionally, the protein levels of p-PI3K (Fig. 6N), p-Akt (Fig. 6O), and p-mTOR (Fig. 6P), the three fundamental biomarkers of cell stress and proliferation signaling, displayed the opposite trend as that observed following oxidative stress among the groups.

Fig. 6 Ove-PrP^C in ADMSCs repressed oxidative stress-induced protein levels of cell senescence, DNA and mitochondrial damage, and upregulated cell proliferation and cell cyclins. (A) Protein expression of cellular prion protein (PrP^C), * vs. †, $P<0.005$. (B) Protein expression of Ki67, * vs. †, $P<0.005$. (C) Protein expression of NOX1, * vs. other groups with different symbols (†, ‡, §), $P<0.001$. (D) Protein expression of NOX-4, * vs. other groups with different symbols (†, ‡, §), $P<0.001$. (E) Protein expression of cyclophilin D, * vs. other groups with different symbols (†, ‡, §), $P<0.0001$. (F) Protein expression of p-DRP1, * vs. other groups with different symbols (†, ‡, §), $P<0.001$. (G) Protein expression of cleaved caspase3, * vs. other groups with different symbols (†, ‡, §), $P<0.001$. (H) Protein expression of cleaved PARP, * vs. other groups with different symbols (†, ‡, §), $P<0.001$. (I) Protein expression of Bax, * vs. other groups with different symbols (†, ‡, §), $P<0.001$. (J) Protein expression of cyclinD1, * vs. other groups with different symbols (†, ‡, §), $P<0.001$. (K) Protein expression of cyclinE1, * vs. other groups with different symbols (†, ‡, §), $P<0.0001$. (L) Protein expression of cdk2, * vs. other groups with different symbols (†, ‡, §), $P<0.001$. (M) Protein expression of cdk4, * vs. other groups with different symbols (†, ‡, §), $P<0.001$. (N) Protein expression of p-PI3K, * vs. other groups with different symbols (†, ‡), $P<0.001$. (O) Protein expression of p-Akt, * vs. other groups with different symbols (†, ‡), $P<0.001$. (R) Protein expression of p-mTOR, * vs. other groups with different symbols (†, ‡, §), $P<0.0001$. All statistical analyses were performed by one-way ANOVA, followed by Bonferroni multiple comparison post hoc test (n = 3 for each group). Symbols (*, †, ‡) indicate significance (at 0.05 level). ADMSCs = adipose-derived mesenchymal stem cells; Ove-PrP^C = overexpression of cellular prion protein. C1 = ADMSCs, C2 = Ove-PrP^C in ADMSCs, C3 = ADMSCs + H_2O_2, C4 = Ove-PrP^C in ADMSCs + H_2O_2

Ove-PrP.^{C} in ADMSCs and mitochondrial treated N2a cells/ρ0 cells upregulated cell viability (Fig. 7)

To evaluate whether Ove-PrP^C of ADMSCs protects the cells against H_2O_2-induced cell growth inhibition, the cells were classified as C1–C4. The MTT assay demonstrated that cell viability was lowest in C3, highest in C2, and significantly higher in C4 than in C1 at 24 (Fig. 7A), 48 (Fig. 7B), and 72 (Fig. 7C) h.

To determine whether mitochondrial treatment augmented cell viability at 24, 48, and 72 h, an MTT assay was performed, and the cells were categorized into A1–A6. The MTT assay demonstrated that cell viability was lowest in A3, highest in A2, significantly higher in A1 than in A4–A6, significantly higher in A6 than in A4 and A5, and significantly higher in A4 than in A5 at the three time points (Fig. 7D–F).

Ex.^{Mito} delivery to N2a (recipient) cells upregulated cell cycle activation and cell proliferation (Fig. 8)

To verify whether mitochondrial treatment accelerated the cell cycle and cell proliferation at the molecular level, western blot analysis was performed. The results showed that the protein expressions of PCN (Fig. 8A) and Ki67 (Fig. 8C), two indicators of cell proliferation, and the protein expression of Cyclin E1 (Fig. 8B), Cyclin D1 (Fig. 8D), Cdk2 (Fig. 8E), and Cdk4 (Fig. 8F), four biomarkers of the cell cycle, were lowest in A3 and A5, highest in A1 and A2, and notably higher in A4 than in A6. These findings suggest that the exogenous energy supply by Ex^{Mito} accelerated the cell cycle and proliferation.

Identification of hemorrhagic area by day 14 after ICH induction and time course of neurological function assessed in the corner test (Fig. 9)

First, to evaluate whether early treatment attenuated the early stage of ICH, whole-brain cross-sections were stained with 3,5-triphenyl-2H-tetrazolium chloride (TTC) on day 14 after ICH induction (Fig. 9A–E). The results demonstrated that the total ICH area was lowest in group 1 (sham-operated control; SC), highest in group 2 (ICH only), and significantly lower in group 5 (IHC + combined Ex^{Mito} + Ove-PrP^C-ADMSCs) than in groups 3 (ICH + Ex^{Mito}) and 4 (ICH + Ove-PrP^C-ADMSCs); there was no difference between groups 3 and 4 (Fig. 9F).

Next, to verify the impact of these therapeutic regimens on neurological functional integrity, the time course of the corner test was evaluated in each animal group (Fig. 9G). The results showed that on day 0 (Fig. 9H) prior to ICH induction, neurological function was similar among the five groups. However, by day 3 (Fig. 9I), neurological function was significantly impaired in groups 2–5 compared to that in group 1; groups 2–5 showed no significant differences. Additionally, on days 7 (Fig. 9J), 14 (Fig. 9K), and 28 (Fig. 9L), neurological function was significantly impaired in group 2 compared to that in group 1, whereas this parameter was significantly progressively improved in groups 3 and 4 and further improved in group 5, highlighting that combined regimens can treat ICH (Fig. 9J–L).

Brain infarct area (IA), brain hemorrhagic volume (BHV) and cellular expression of neurons by day 28 after ICH induction (Fig. 10)

Hematoxylin and eosin staining was performed to evaluate the brain IA at the end of the study period (Fig. 10A–E). The results showed that the IA was lowest in group 1, highest in group 2, and significantly lower in group 5 than in groups 3 and 4; however, there was no difference between groups 3 and 4 (Fig. 9F).

To further verify the anatomical integrity of the brain parenchyma, we performed brain magnetic resonance imaging (MRI) (Fig. 10G–K). As expected, by day 28 of IHC induction, brain MRI demonstrated that the summation of the BHV exhibited an identical pattern as brain IA among all groups (Fig. 10L).

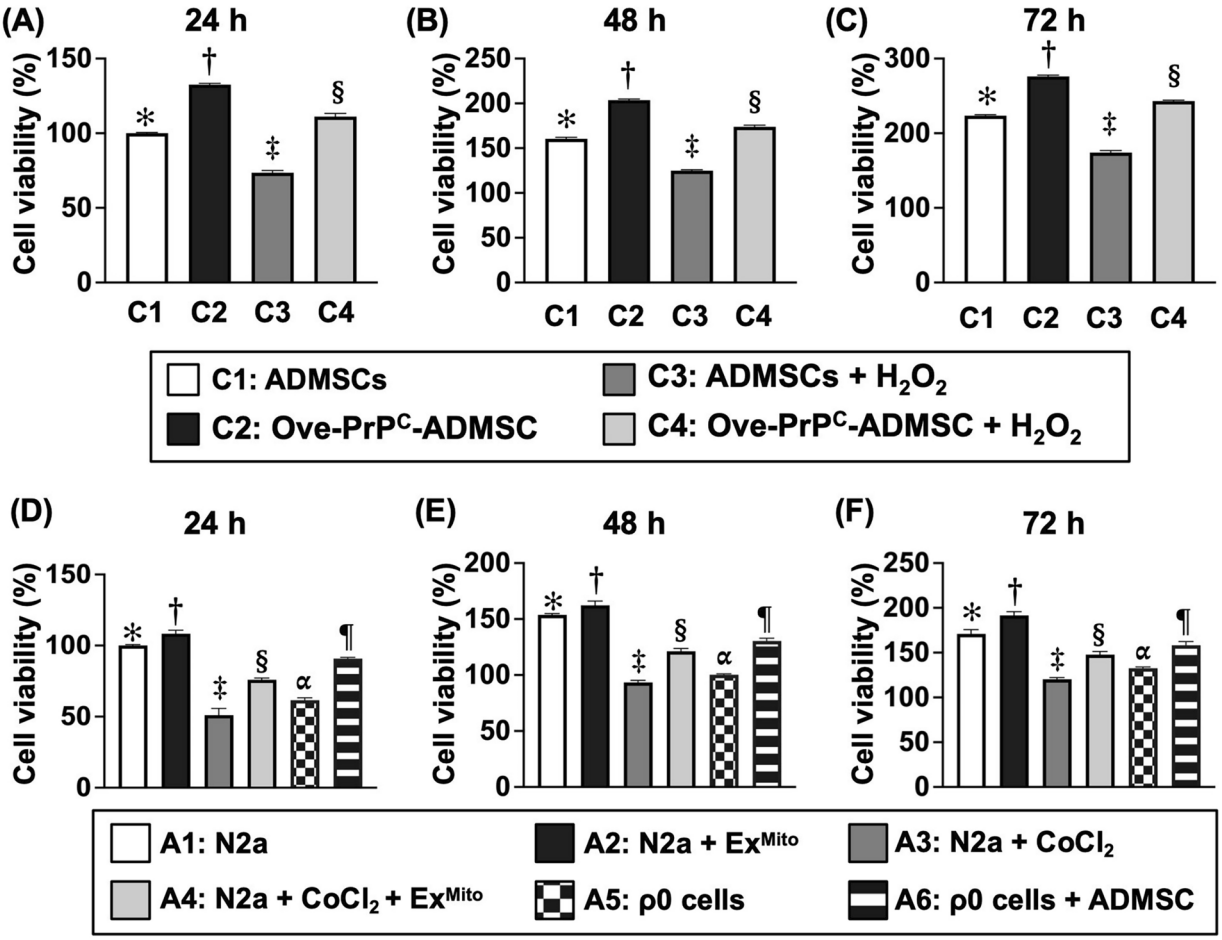

Fig. 7 Ove-PrP^C in ADMSCs treated N2a cells/ρ0 cells upregulated the cell viability. (A) ADMSCs viability at 24 h, * vs. other groups with different symbols (†, ‡, §), $P<0.0001$. (B) ADMSCs viability at 48 h, * vs. other groups with different symbols (†, ‡, §), $P<0.0001$. (C) ADMSCs viability at 72 h, * vs. other groups with different symbols (†, ‡, §), $P<0.0001$. C1 = ADMSCs, C2 = Ove-PrP^C in ADMSCs, C3 = ADMSCs + H_2O_2, C4 = Ove-PrP^C in ADMSCs + H_2O_2. (D) N2a/ρ0 cell viability at 24 h, * vs. other groups with different symbols (†, ‡, §, ¶, α), $P<0.0001$. (E) N2a/ρ0 cell viability at 48 h, * vs. other groups with different symbols (†, ‡, §, ¶, α), $P<0.0001$. (F) N2a/ρ0 cell viability at 72 h, * vs. other groups with different symbols (†, ‡, §, ¶, α), $P<0.0001$. A1 = N2a cells, A2 = N2a cells + Ex^{Mito}, A3 = N2a cells + $CoCl_2$, A4 = N2a + $CoCl_2$ + Ex^{Mito}, A5 = ρ0 cells, A6 = ρ0 cells + ADMSCs. All statistical analyses were performed by one-way ANOVA, followed by Bonferroni multiple comparison post hoc test (n = 6 for each group). Symbols (*, †, ‡, §, ¶, α) indicate significance (at 0.05 level). ADMSCs = adipose-derived mesenchymal stem cells; Ove-PrP^C = overexpression of cellular prion protein

To clarify the molecular-level brain microstructural integrity of these animals, IF microscopic evaluations were conducted (Fig. 10M–Q). The number of NeuN + cells, an index of neurons, was highest in group 1, lowest in group 2, and significantly higher in group 5 than in groups 3 and 4 but did not differ between groups 3 and 4 (Fig. 10R).

Cellular levels of inflammation and DNA damage in brain hemorrhagic region by day 28 after ICH induction (Fig. 11)

At the cellular level, the expression of CD68 (Fig. 11A–E), an index of inflammation, and expression of γ-H2AX (Fig. 11G–K), a DNA-damaged biomarker, were lowest in group 1, highest in group 2 and significantly lower in group 5 than in groups 3 and 4 but did not differ between groups 3 and 4 (Fig, 11F, L).

Expression of cell cycle and cell stress signaling proteins in the brain tissue at day 28 after ICH induction (Fig. 12)

We utilized western blotting to determine the cell cycle, cell stress, and cell proliferation signaling molecule levels. The protein levels of Cyclin D1 (Fig. 12A), Cyclin E1 (Fig. 12B), Cdk2 (Fig. 12C), and Cdk4 (Fig. 12D), the four biomarkers of the cell cycle, were highest in group 1, lowest in group 2, and significantly higher in group 5 than in groups 3 and 4; however, they exhibited a similar pattern between groups 3 and 4. Additionally, the protein levels of p-PI3K (Fig. 12E),

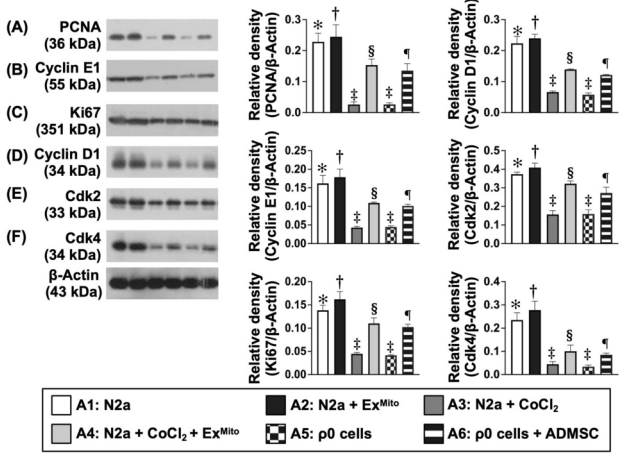

Fig. 8 Ex^{Mito} delivery to N2a (recipient) cells upregulated the cell cycle activation and cell proliferation. (A) Protein expression of PCN, * vs. other groups with different symbols (†, ‡, §, ¶), $P<0.001$. (B) Protein expression of Ki67, * vs. other groups with different symbols (†, ‡, §, ¶), $P<0.001$. (C) Protein expression of cyclin D1, * vs. other groups with different symbols (†, ‡, §, ¶), $P<0.001$. (D) Protein expression of cyclin E1, * vs. other groups with different symbols (†, ‡, §, ¶), $P<0.001$. (E) Protein expression of cdk2, * vs. other groups with different symbols (†, ‡, §), $P<0.001$. (F) Protein expression of cdk4, * vs. other groups with different symbols (†, ‡, §, ¶), $P<0.001$. A1 = N2a cells, A2 = N2a cells + exogenous mitochondria, A3 = N2a cells + $CoCl_2$, A4 = N2a + $CoCl_2$ + exogenous mitochondria, A5 = ρ0 cells, A6 = ρ0 cells + ADMSCs. All statistical analyses were performed by one-way ANOVA, followed by Bonferroni multiple comparison post hoc test (n = 6 for each group). Symbols (*, †, ‡, §, ¶, α) indicate significance (at 0.05 level). ADMSCs = adipose-derived mesenchymal stem cells

p-Akt (Fig. 12F), and p-mTOR (Fig. 12G), three biomarkers of cell stress and cell survival signaling, were progressively significantly increased from groups 1 to 5, indicating that these factors were activated under ischemic conditions, further upregulated by Ex^{Mito} and Ove-PrP^{C}-ADMSCs treatments, and further upregulated by a combination of the two regimens.

Expression of oxidative stress, mitochondrial damage, DNA damage, apoptosis, and fibrosis proteins in the brain tissue at day 28 after ICH induction (Fig. 13)

Finally, to verify that cell damage markers were attenuated by Ex^{Mito} and Ove-PrP^{C}-ADMSCs treatment, western blot analysis was performed. As expected, the protein expressions of NOX-1 (Fig. 13A) and NOX-4 (Fig. 13C), two indices of oxidative stress; protein expression of p-DRP1 (Fig. 13F), PINK (Fig. 13G) and γ-H2AX (Fig. 13B), three indices of mitochondrial-DNA damaged biomarkers; protein expressions of mitochondrial Bax (Fig. 13H), cleaved caspase3 (Fig. 13D) and cleaved PARP (Fig. 13E), three indices of apoptosis; and protein expressions of p-Smad3 (Fig. 13I) and TGF-β (Fig. 13J), two indices of fibrosis, were lowest in group 1, highest in group 2 and significantly lower in groups 5 than in groups 3 and 4 but did not differ between the latter two groups (Fig. 14).

Ove-PrP^{C} in ADMSCs alleviated apoptosis, autophagy, and mitochondrial damage (Supplementary Fig. 1)

To examine whether Ove-PrP^{C} in ADMSCs could repress the hypoxia-induced cell damage at the molecular level, the cells were categorized into D1 (ADMSCs), D2 [ADMSCs + $CoCl_2$ (100 μM for 24 h)], D3 (Ove-PrP^{C} in ADMSCs), and D4 (Ove-PrP^{C} in ADMSCs + $CoCl_2$), and western blot analysis was performed. The results showed that the protein expression of cleaved capase3 (Supp. Figure 1A), cleaved PARP (Supp. Figure 1B), and Bax (Supp. Figure 1C) (three indices of apoptosis); Beclin1 (Supp. Figure 1D), Atg5 (Supp. Figure 1E) and the ratio of LC3B-II to LC3B-I (Supp. Figure 1F) (three indicators of autophagy); and p-DRP1 (Supp. Figure 1G) and cyclophilin D (Supp. Figure 1H) (two indices of mitochondrial damage) were lowest in D3, highest in D2, and significantly higher in D4 than in D1.

Discussion

We performed a preclinical investigation to explore the effect of combined Ex^{Mito} and Ove-PrP^{C} in ADMSCs treatment. First, the combined regimen was superior to the single regimen in reducing the ICH volume and infarct size. Second, importantly, in rats with ICH, neurological outcomes were significantly improved by both treatments and further significantly improved by combined Ex^{Mito} and Ove-PrP^{C} in ADMSCs treatment. Third, at the molecular-cellular levels, these therapeutic regimens improved outcomes mainly by reducing oxidative stress, mitochondrial damage, and inflammation, along with activating the cell cycle and proliferation.

Compared with untreated IHC animals, the Ex^{Mito} or Ove-PrP^{C} in ADMSCs treatments reduced the BHV and brain IA, resulting in improved neurological function in animals with ICH. Considerably, our previous study demonstrated that exogenous mitochondrial transfusion significantly protected the liver against ischemia–reperfusion injury, mainly by repressing mitochondrial permeability transition in rodents (Chen et al. 2023). Additionally, our recent study demonstrated that Ove-PrP^{C} in ADMSCs therapy attenuated spinal cord injury in rats (Chen et al. 2016b). Accordingly, our findings are comparable with those of our previous studies (Chen et al. 2023, 2016b). The most important finding

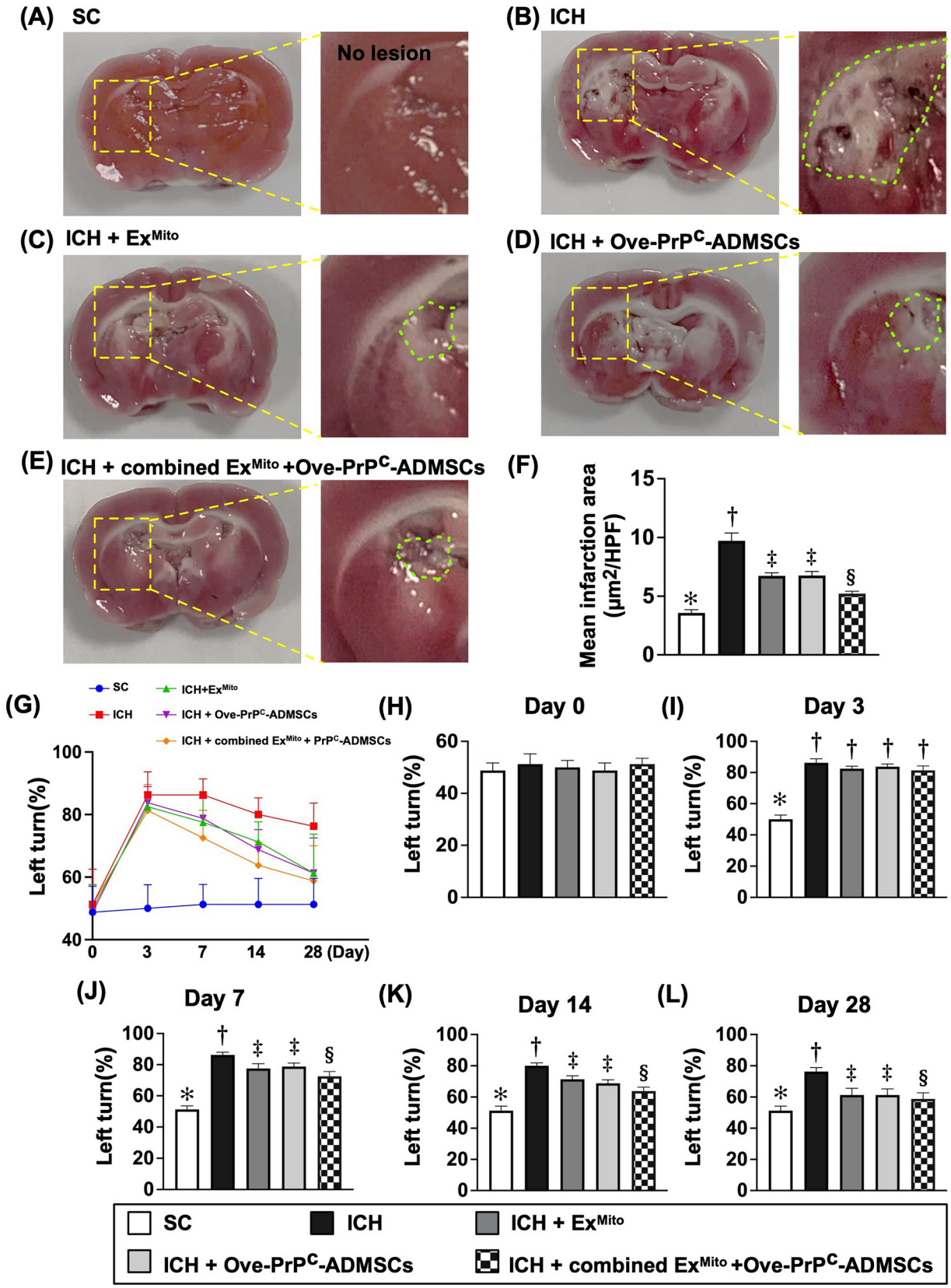
(A) SC
No lesion
(B) ICH
(C) ICH + ExMito
(D) ICH + Ove-PrPC-ADMSCs
(E) ICH + combined ExMito +Ove-PrPC-ADMSCs
(F)
Mean infarction area (μm2/HPF)
(G)
SC
ICH
ICH+ExMito
ICH + Ove-PrPC-ADMSCs
ICH + combined ExMito + PrPC-ADMSCs
Left turn(%)
0 3 7 14 28 (Day)
(H) Day 0
(I) Day 3
(J) Day 7
(K) Day 14
(L) Day 28
SC
ICH
ICH + ExMito
ICH + Ove-PrPC-ADMSCs
ICH + combined ExMito +Ove-PrPC-ADMSCs

Fig. 9 Identification of hemorrhagic area by day 14 after ICH induction and time courses of neurological function assessed by corner test. (A–E) Illustrating the TTC stain for identification of the brain hemorrhagic area. Note that "a, b, c and d" indicated the manifestation of square area in A, B, C, D and E, respectively. (F) Analytical result of hemorrhagic area (green dotted line in large square, * vs. other groups with different symbols (†, ‡, §), $P<0.001$. (G) Schematically illustrated the time courses of the changes of neurological function. (H) Neurological function (i.e., by Corner Test) at day 0 $p>0.5$. (I) Neurological function by day 3, * vs. †, $P<0.0001$. (G) Neurological function by day 7, * vs. other groups with different symbols (†, ‡), $P<0.001$. (K) Neurological function by day 14, * vs. other groups with different symbols (†, ‡, §, ¶), $P<0.001$. (K) Neurological function by day 28, * vs. other groups with different symbols (†, ‡, §), $P<0.001$. All statistical analyses were performed by one-way ANOVA, followed by Bonferroni multiple comparison post hoc test (n = 6–10 for each group). Symbols (*, †, ‡, §, ¶) indicate significance (at 0.05 level). ADMSCs = adipose-derived mesenchymal stem cells. Overexpression of cellular prion protein (Ove-PrP^C). Group 1 = sham-operated control (SC); group 2 = intracranial hemorrhage (ICH); group 3 = ICH + Ex^{Mito}; group 4 = ICH + Ove-PrP^C-ADMSCs; group 5 = IHC + combined Ex^{Mito} + Ove-PrP^C-ADMSCs

was that combined therapy with these two regimens further reduced the BHV and brain IA and improved neurological function compared with the effects of only one therapy. Thus, our findings extend those of previous studies (Chen et al. 2023, 2016b).

The underlying mechanism of neuron/brain parenchymal damage in stroke settings, such as ischemic stroke or ICH, is complicated (Chen et al. 2014a; Hostettler et al. 2019; Haupenthal et al. 2021; Gaiqing 2014; Duan et al. 2016; Shao et al. 2019; Yip et al. 2020). However, the abrupt loss of blood supply due to vessel occlusion or compression by a hematoma always results in a rigorous inflammatory reaction, generation of oxidative stress, and mitochondrial damage, which is universally accepted as the main cause of neuron/brain parenchymal damage. Our results demonstrate that these parameters were remarkably enhanced in rats after ICH. Accordingly, our findings corroborate those of previous studies (Chen et al. 2014a; Hostettler et al. 2019; Haupenthal et al. 2021; Gaiqing 2014; Duan et al. 2016; Shao et al. 2019; Yip et al. 2020). Particularly, inflammation and mitochondrial damage were markedly reversed by mitochondria or Ove-PrP^C in ADMSCs and further reversed by combined Ex^{Mito} and Ove-PrP^C in ADMSCs treatment. Thus, our findings, in addition to those of previous studies (Chen et al. 2014a; Hostettler et al. 2019; Haupenthal et al. 2021; Gaiqing 2014; Duan et al. 2016; Shao et al. 2019; Yip et al. 2020), partly explain why the BIV and brain IA were notably reduced and neurological function (i.e., corner test) was notably improved in ICH rats after receiving mitochondria-Ove-PrP^C in ADMSCs treatment.

Notably, our study, including both in vitro and in vivo findings consistently revealed that cell cycle parameters were substantially upregulated following treatment with mitochondria or Ove-PrP^C in ADMSCs, thereby enhancing cell viability and promoting proliferation. In addition, one attractive finding was that NOX/cell-stress signaling which was involved in neuronal death following ICH was remarkably attenuated by Ove-PrP^C in ADMSCs treatment, suggesting that this PrP^C gene activation in ADMSCs has antioxidant capacity. Perhaps, this finding could be explained as the results of this gene manipulation ensured the Ove-PrP^C in ADMSCs survival in ischemic environment to offer great ability for alleviating the oxidative stress induced cerebral tissue damage.

One interesting finding in the in vitro study was that the mitochondria could be donated from abundant mitochondria of ADMSCs (i.e., donor) to mitochondrial deprived neurons (ρ0 cells) (recipient), i.e., just likes a similar phenomenon of blood transfusion in human being. This phenomenon could be extrapolated to the in vivo study that the mitochondria derived from Ove-PrP^C in ADMSCs could be transferred to ischemic neuronal cells (recipient) in setting of IHC. This novel finding could, at least in part, explained why the Ex^{Mito}/Ove-PrP^C in ADMSCs treatment effectively reduced the infarct area/infarct volume and improved neurological outcomes. This may also be one of the fundamental mechanisms by which Ex^{Mito} treatment protects brain neurons against the abrupt loss of blood supply after ICH.

Study limitations

Our study had some limitations. First, although Ex^{Mito} and Ove-PrP^C in ADMSCs treatments showed promising results in this preclinical study, ethical considerations may arise when applying this therapeutic strategy to clinical settings for patients with ICH. Second, the mechanisms underlying neuronal damage and neurological dysfunction following ICH are complex and warrant further analysis. Figure 13 provides a schematic illustration of underlying mechanism of ICH-induced neuronal death, impaired neurological function, and the proposed treatment approach based on our findings.

In conclusion, our results show that inflammation, oxidative stress, and mitochondrial damage are the primary factors that induce brain damage after ICH. The combination of Ex^{Mito} and PrP^{C-OE} in ADMSCs exerted a synergistic effect in protecting the brain from ICH damage.

Experimental procedures

Ethical issues

All animal procedures were approved by the Institute of Animal Care and Use Committee at Kaohsiung Chang Gung Memorial Hospital (Affidavit of Approval of Animal Use

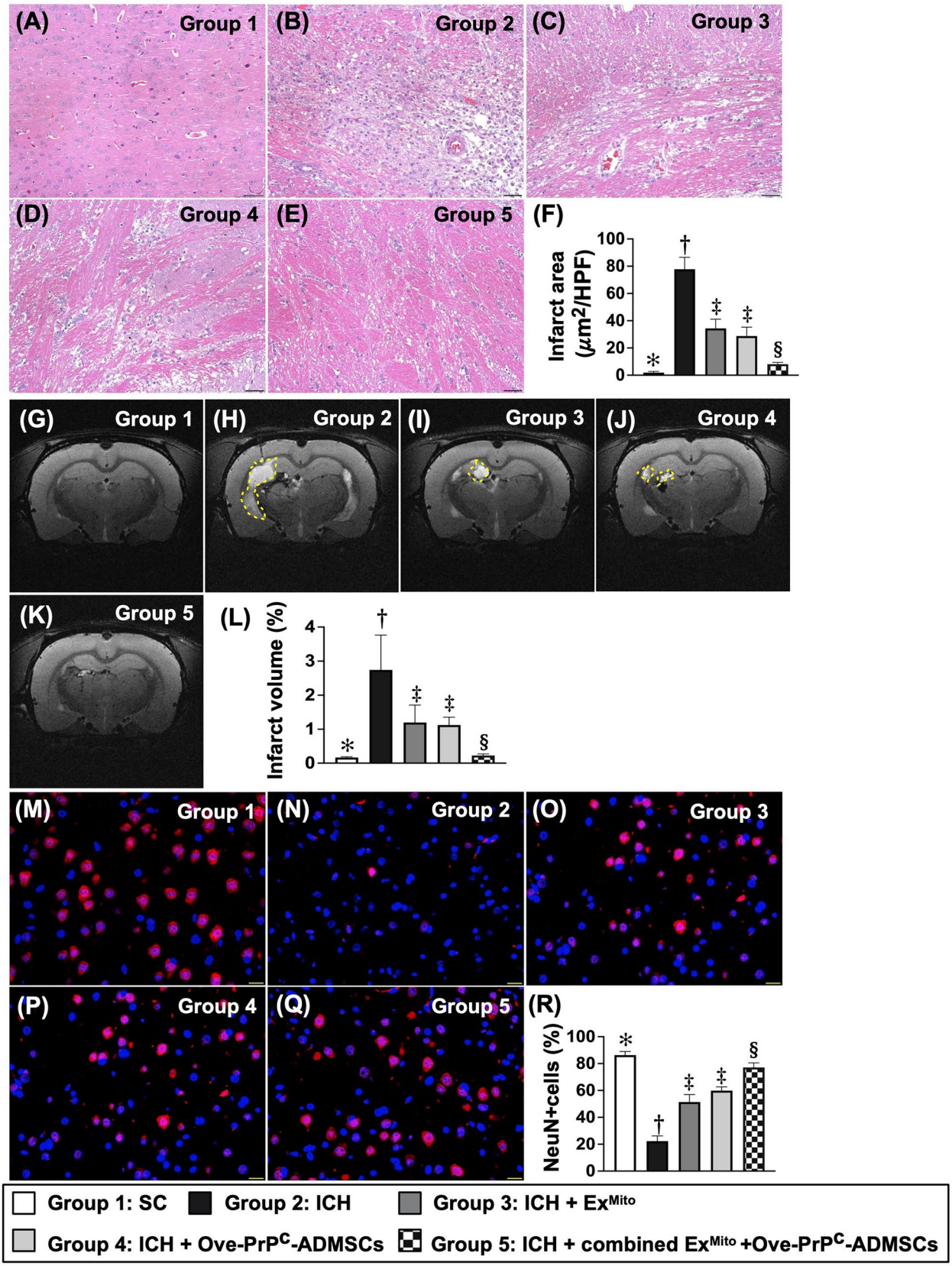
(A) Group 1
(B) Group 2
(C) Group 3
(D) Group 4
(E) Group 5
(F)
Infarct area (μm2/HPF)
100
80
60
40
20
0
*
†
‡
‡
§
(G) Group 1
(H) Group 2
(I) Group 3
(J) Group 4
(K) Group 5
(L)
Infarct volume (%)
4
3
2
1
0
*
†
‡
‡
§
(M) Group 1
(N) Group 2
(O) Group 3
(P) Group 4
(Q) Group 5
(R)
NeuN+cells (%)
100
80
60
40
20
0
*
†
‡
‡
§
Group 1: SC
Group 2: ICH
Group 3: ICH + ExMito
Group 4: ICH + Ove-PrPC-ADMSCs
Group 5: ICH + combined ExMito +Ove-PrPC-ADMSCs

Fig. 10 Brain infarct area, brain hemorrhagic volume (BHV) and cellular expression of neurons by day 28 after ICH induction. (A–E) Illustrating the microscopic finding (200x) of H.E., stain for identification of infarct area at the same level of cerebral cross sections (whitish area). Scale bar in right lower corner represents 50 µm. (F) Analytical result of brain infarct area, * vs. other groups with different symbols (†, ‡, §), $P<0.0001$. (G–K) Illustrating the brain magnetic resonance imaging (MRI) finding for identification of brain hemorrhagic zone (white color) (yellow dotted-line area). (L) Analytical result of brain hemorrhagic volume (i.e., the percentage of the whole brain volume), * vs. other groups with different symbols (†, ‡, §), $P<0.0001$. (M–Q) Illustrating the immunofluorescent (IF) microscopic finding (400x) for identification of cellular expression of NeuN cells (red color). Scale bar in right lower corner represents 20 µm. (R) Analytical result of number of NeuN+cells, * vs. other groups with different symbols (†, ‡, §), $P<0.0001$. All statistical analyses were performed by one-way ANOVA, followed by Bonferroni multiple comparison post hoc test (n=8–10 for each group). Symbols (*, †, ‡, §) indicate significance (at 0.05 level). ADMSCs=adipose-derived mesenchymal stem cells. Ove-PrP^C=Overexpression of cellular prion protein

Protocol No. 2021120204) and were performed in accordance with the Guide for the Care and Use of Laboratory Animals.

Animals were housed in an Association for Assessment and Accreditation of Laboratory Animal Care International (AAALAC; Frederick, MD, USA)-approved animal facility in our hospital with controlled temperature and light cycles (24 °C and 12-h/12-h light cycle).

Preparation of $CoCl_2$ stock solution and hypoxia treatment

The procedure and protocol were based on a previous report (Yin et al. 2023) with minimal modifications. A stock solution 25 mM of cobalt chloride ($CoCl_2$) was prepared in sterile distilled water and diluted in medium to obtain the final concentrations. The N2a cell line was cultured in Dulbecco's modified Eagle's medium (DMEM)supplemented with 10% fetal bovine serum (FBS), 100 U/mL penicillin, and 100 µg/mL streptomycin in a standard CO_2 incubator. After 24 h, the N2a cells were treated with $CoCl_2$ (i.e., 100 µM) co-culture for 24 h.

Mitochondrial isolation from donors and MitoTracker staining for mitochondria

Liver mitochondria were isolated from donor Sprague–Dawley rats, as previously described (Rana et al. 2019). The rats were fasted overnight prior to the mitochondrial isolation procedure and euthanized, and their gallbladders and livers were carefully isolated and removed. Briefly, the liver (3–5 g) was immersed in 100 mL ice-cold IBc (10 mM Tris–MOPS, 5 mM EGTA/Tris, and 200 mM sucrose, pH 7.4) in a beaker, followed by rinsing to remove the blood with ice-cold IBc. The liver was minced using scissors in a beaker containing ice. IBc was discarded during mincing and replaced with 18 mL of ice-cold fresh IBc. The livers were homogenized using a Teflon pestle. The homogenates were transferred to a 50-mL polypropylene Falcon tube and centrifuged at 600×*g* for 10 min at 4 °C. The supernatants were transferred to fresh tubes for centrifugation at 7,000×*g* for 10 min at 4 °C. The supernatants were discarded, and the pellets were washed with 5 mL of ice-cold IBc. The supernatants from the pellets were centrifuged at 7,000×*g* for 10 min at 4 °C. The supernatants were discarded and the pellets containing mitochondria were resuspended. The concentration of the mitochondrial suspension was measured using the biuret method. Isolated mitochondria (10 mg) were labeled with 1 M MitoTracker Red CMXRos (Invitrogen, Carlsbad, CA, USA) and incubated at 37 °C for 30 min. Finally, exogenous mitochondria (Ex^{Mito}) were co-cultured with healthy and hypoxic N2a cells, and mitochondrial transfusion into the study animals was performed immediately after labeling (<3 h after the isolation procedure).

Preparation of N2a cell line

Neuro-2a cells (N2a: neuroblastoma cell line) were maintained in minimum essential medium supplemented with 10% fetal bovine serum, 2 mM L-glutamine, 0.1 mM non-essential amino acids, 1.0 mM sodium pyruvate, 100 U/mL penicillin G, and 100 µg/mL streptomycin. To create mitochondrial-DNA depleted cells (i.e., ρ0 cells) of N2a, the N2a cells were incubated with ethidium bromide (0.5 µg/mL) for 2 weeks to influence mitochondrial DNA replication. Throughout the experimental period, ρ0 and N2a cells were grown in minimum essential medium supplemented with 50 µg/mL uridine.

Measurement of mitochondrial OCR

Mitochondrial bioenergetics in N2a cells under different conditions were determined using an Extracellular Flux Analyzer (XFe24 Seahorse Bioscience, North Billerica, MA, USA) by assessing mitochondrial oxygen consumption, basal respiration, maximal respiration, ATP production, and spare respiratory capacity. Briefly, N2a cells (10^4 cells/per well) were seeded into FBS-free and sodium bicarbonate-free DMEM (high-glucose). During the reactions, 100 µM oligomycin, 100 µM FCCP and 540 µL antimycin A/rotenone were added sequentially. The OCR was measured sequentially (Fig. 1).

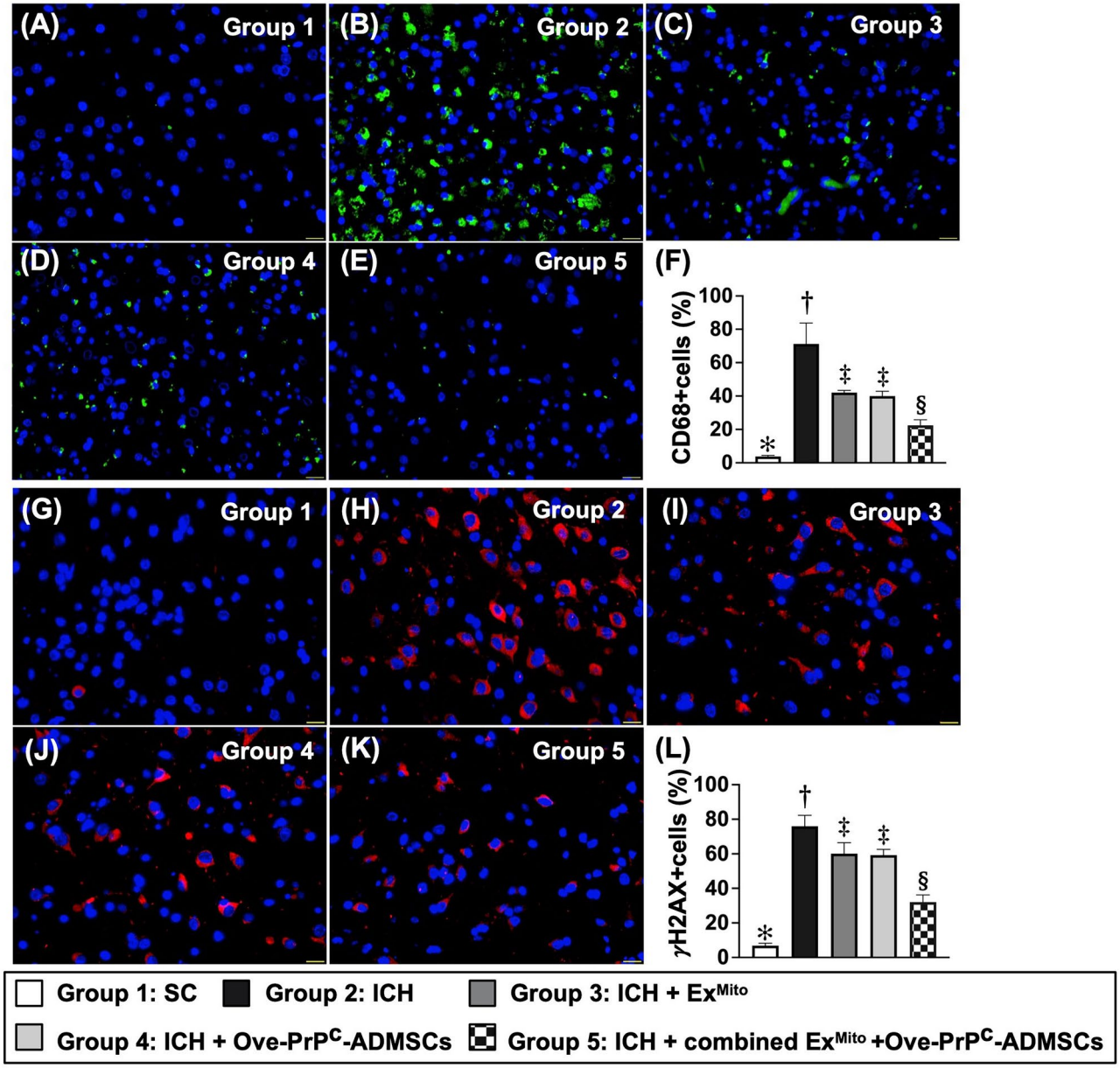

Fig. 11 Cellular levels of inflammation and DNA damage in brain hemorrhagic region by day 28 after ICH induction. (A–E) Illustrating the IF microscopic finding (400x) for identification of cellular expression of CD68 (green color). (F) Analytical result of number of CD68 + cells, * vs. other groups with different symbols (†, ‡, §), $P < 0.0001$. (G–K) Illustrating the IF microscopic finding (400x) for identification of cellular expression of γ-H2AX (red color). (L) Analytical result of number of γ-H2AX + cells, * vs. other groups with different symbols (†, ‡, §), $P < 0.0001$. All statistical analyses were performed by one-way ANOVA, followed by Bonferroni multiple comparison post hoc test (n = 8 for each group). Symbols (*, †, ‡, §) indicate significance (at 0.05 level). ADMSCs = adipose-derived mesenchymal stem cells. Ove-PrP^C = overexpression of cellular prion protein

Preparation of allogenous adipose tissue for culturing ADMSCs

To prepare autologous ADMSCs, the adipose tissue was isolated from 12 rats. The procedure and protocol for ADMSCs preparation are described in our previous reports (Weissmann 2004; Chen et al. 2014b, 2016a; Lin et al. 2016). Briefly, adipose tissue surrounding the epididymis was carefully dissected, excised, and processed. Following standardized preparation steps (Weissmann 2004; Chen et al. 2014b, 2016a; Lin et al. 2016), the cells were resuspended in saline. An aliquot of this cell suspension was cultured in low-glucose (DMEM)-with 10% FBS for 14 days. Approximately $2–3 \times 10^6$ ADMSCs were obtained per rat.

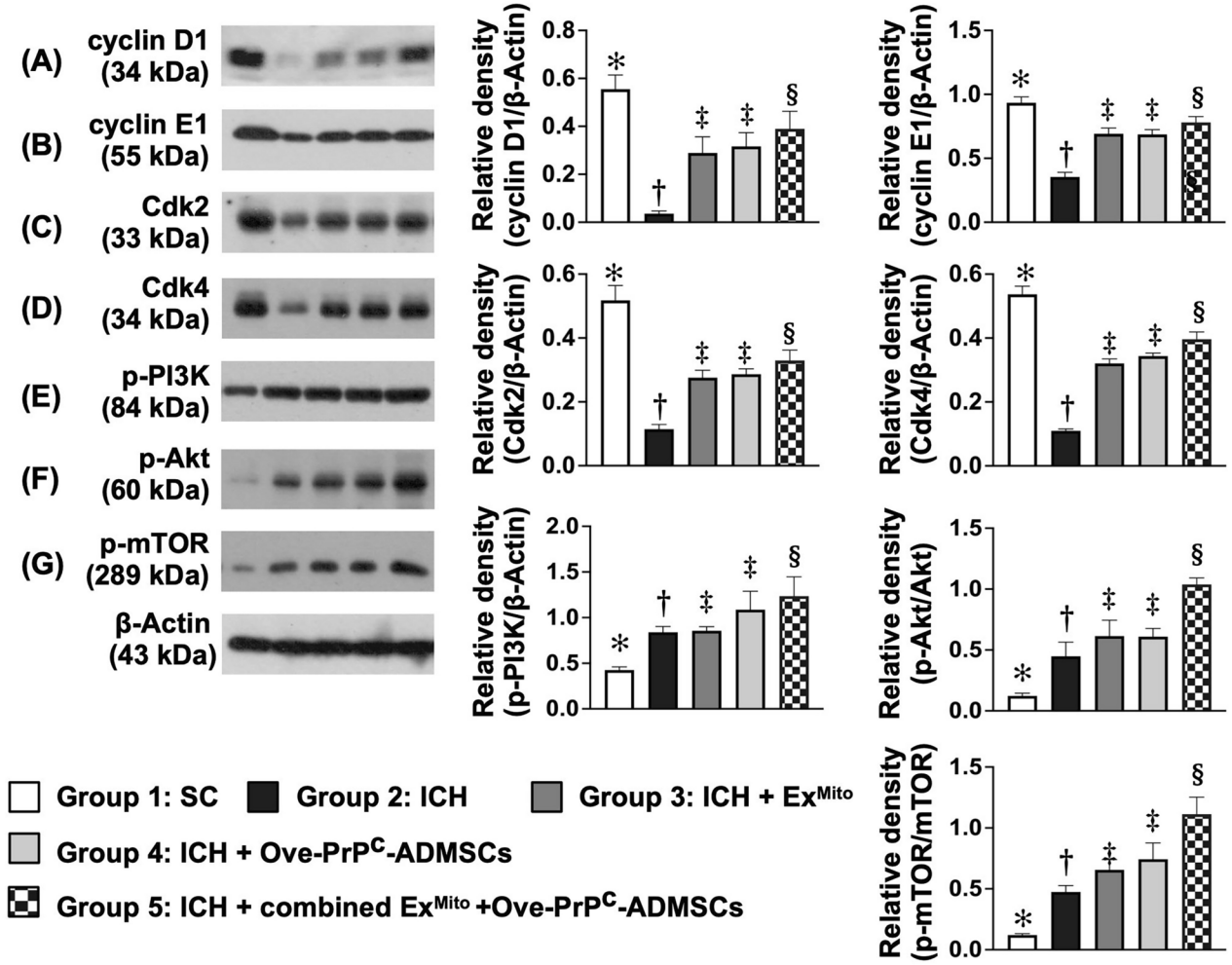

Fig. 12 Protein expressions of cell cycle and cell stress signaling in the brain tissue by day 28 after ICH induction. (A) Protein level of cyclin D1, * vs. other groups with different symbols (†, ‡, §), $P<0.0001$. (B) Protein expression of cyclin E1, * vs. other groups with different symbols (†, ‡, §), $P<0.0001$. (C) Protein expression of cdk2, * vs. other groups with different symbols (†, ‡, §), $P<0.0001$. (D) Protein expression of cdk4, * vs. other groups with different symbols (†, ‡, §), $P<0.0001$. (E) Protein expression of p-PI3K, * vs. other groups with different symbols (†, ‡, §), $P<0.0001$. (F) Protein expression of p-Akt, * vs. other groups with different symbols (†, ‡, §), $P<0.0001$. (G) Protein expression of p-mTOR, * vs. other groups with different symbols (†, ‡, §), $P<0.0001$. All statistical analyses were performed by one-way ANOVA, followed by Bonferroni multiple comparison post hoc test (n = 6 for each group). Symbols (*, †, ‡, §) indicate significance (at 0.05 level). ADMSCs = adipose-derived mesenchymal stem cells. Ove-PrP^C = overexpression of cellular prion protein

Transfection of ADMSCs with plasmids for PrP^C overexpression (Ove-PrP.^{C})

The procedure and protocol were reported in our recent study (Yip et al. 2021b). The pCS6-*PRNP* plasmid was purchased from Transomics Technologies (Huntsville, Alabama, USA). Briefly, plasmid transfection was performed using Lipofectamine 3000 (Invitrogen, Life technologies, Carlsbad, CA, USA) according to the manufacturer's instructions with slight modifications. The cells were replated 24 h before transfection at a density of 5×10^5 cells in 4 mL of fresh culture medium in a 6-cm plastic dish. Briefly, 10 µg of the *PRNP* expression vector and 20 µL Lipofectamine 3000 were incubated at room temperature for 15 min, followed by overnight incubation of cells at 37 °C in a humidified atmosphere of 5% CO_2 and Lipofectamine (i.e., mixed together), after which the relevant experiments were carried out.

Cell grouping and verification of cell-to-cell-transferred mitochondria by TNT system

To test whether ADMSCs (i.e., donor) could transfer their mitochondria into hypoxia-treated neuronal cells (i.e., recipient), i.e., "cell-to-cell transfer," we utilized a cell-culture model, and the cells were categorized as follows: A1 (N2a cells), A2 [N2a cells + exogenous mitochondria (100 µg co-cultured for 3 h)], A3 [N2a cells + $CoCl_2$ (100 µM co-culture for 24 h)], A4 (N2a + $CoCl_2$ + exogenous mitochondria), A5

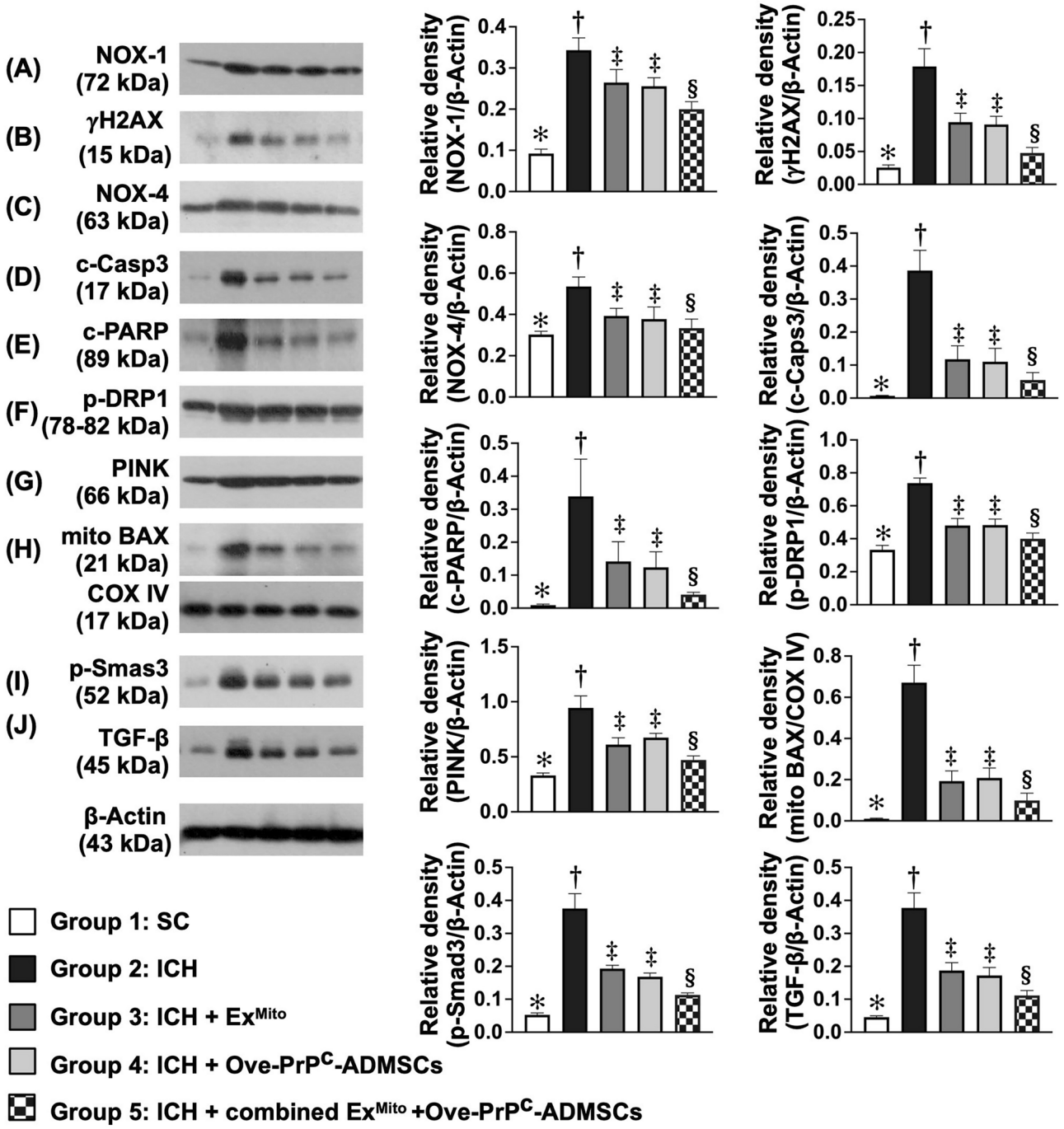

Fig. 13 The protein expressions of oxidative stress, mitochondrial damage, DNA damage apoptosis and fibrosis in the brain tissue by day 28 after ICH induction. (A) Protein expression of NOX-1, * vs. other groups with different symbols (†, ‡, §), $P<0.0001$. (B) Protein expression of NOX-4, * vs. other groups with different symbols (†, ‡, §), $P<0.0001$. C) Protein expression of p-DRP1, * vs. other groups with different symbols (†, ‡, §), $P<0.0001$. (D) Protein expression of PINK, * vs. other groups with different symbols (†, ‡, §), $P<0.0001$. (E) Protein expression of γ-H2AX, * vs. other groups with different symbols (†, ‡, §), $P<0.0001$. (F) Protein expression of mitochondrial Bax, * vs. other groups with different symbols (†, ‡, §), $P<0.0001$. (G) Protein expression of cleaved caspase3, * vs. other groups with different symbols (†, ‡, §), $P<0.0001$. (H) Protein expression of cleaved PARP, * vs. other groups with different symbols (†, ‡, §), $P<0.0001$. (I) Protein expression of p-Smad3, * vs. other groups with different symbols (†, ‡, §), $P<0.0001$. (J) Protein expression of TGF-β, * vs. other groups with different symbols (†, ‡, §), $P<0.0001$. All statistical analyses were performed by one-way ANOVA, followed by Bonferroni multiple comparison post hoc test (n = 6 for each group). Symbols (*, †, ‡, §) indicate significance (at 0.05 level). ADMSCs = adipose-derived mesenchymal stem cells. Ove-PrP^C = overexpression of cellular prion protein

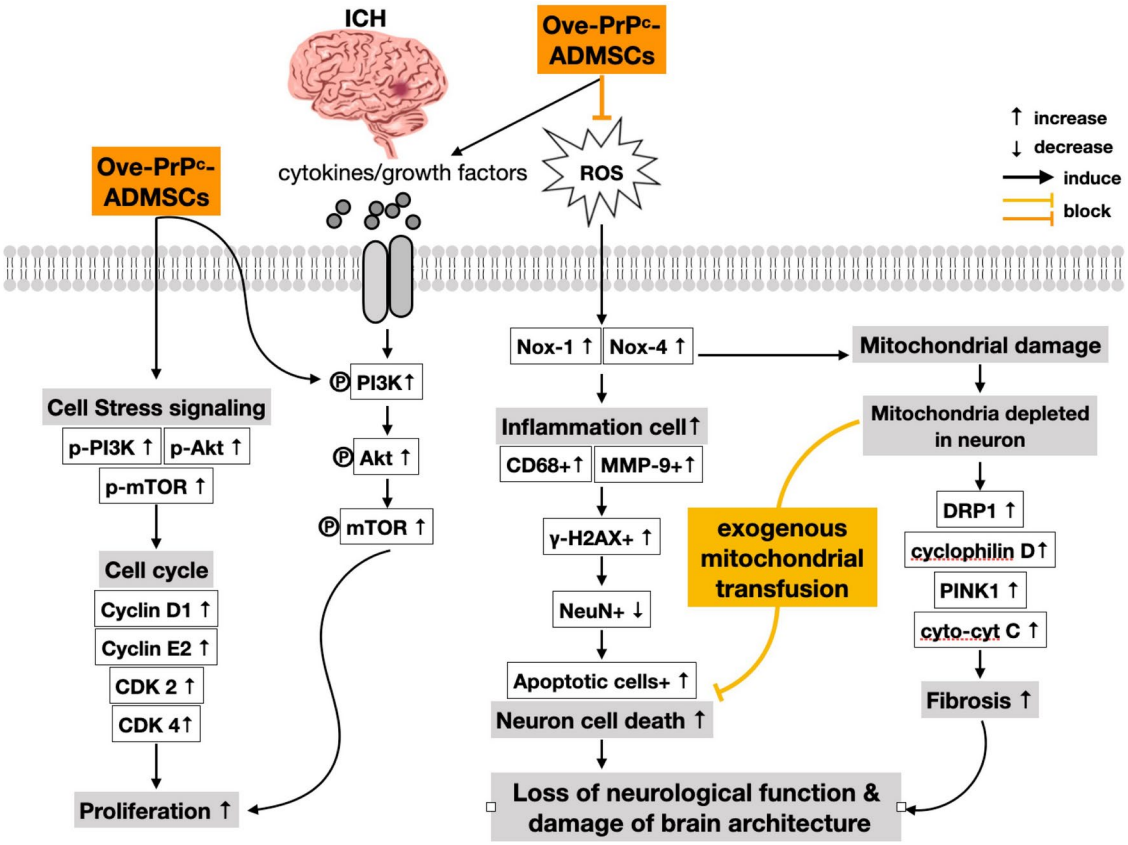

Fig. 14 Schematically illustrated the underlying mechanism of combined Ex^{Mito} and Ove-PrP^{C} in ADMSCs on improving the neurological outcomes in rat after ICH. IHC = intracranial hemorrhage; Ove-PrP^{C} = overexpression of cellular prion protein; Ex^{Mito} = exogenous mitochondria

(ρ0 cells) and A6 (ρ0 cells + ADMSCs). The dose of exogenous mitochondria and procedure and protocol of this experimental study were based on our recent report (Yip et al. 2020).

Additionally, to determine whether ADMSCs (i.e., donor) could transfer their mitochondria into mitochondria-deprived neuronal cells (i.e., recipient), the cells were categorized as follows: B1 (ρ0 cells) and B2 [(ρ0 cells) + ADMSCs], respectively.

Furthermore, to investigate whether Ove-PrP^{C} in ADMSCs upregulates cell proliferation, suppresses oxidative stress, and upregulates cell stress signaling, we used a cell culture model. The cells were categorized as follows: C1 (ADMSCs only), C2 (Ove-PrP^{C} in ADMSCs), C3 [ADMSCs + H_2O_2 (200 μM) treated for 6 h, followed by culture for 18 h], and C4 [Ove-PrP^{C} in ADMSCs + H_2O_2 (200 μM)] treated for 6 h, followed by culture for 18 h]. After culture, the cells were collected for individual studies.

Furthermore, to confirm that the ADMSCs-derived mitochondria (i.e., donor cells) could be transferred into ρ0 cells (mitochondrial-DNA depleted cells) (i.e., recipient cells] through the TNT system, the mitochondria of ADMSCs was first stained by Mitotracker (red color), followed by co-cultured with ρ0 cells. Finally, the cells were collected and under the IF microscopic examination, the TNT system transferred positively MitoTracker-stained mitochondria from ADMSCs (donor) to ρ0 cells (recipient) was clearly identified (referred from Fig. 3).

MTT cell viability assay

The growth of N2a cells was evaluated using the MTT assay. Approximately 2×10^3 cells in 100 μL of medium (stock in 100% ethanol at 100 mM, working concentration of 1 mM) were seeded into the wells of a 96-well plate and incubated for 6 h. The medium was changed, followed by incubation for an additional 24, 48, and 72 h. For the MTT assay, 2000 cells per well were seeded into 96-well plates in 100 μL of medium with or without 50 μM H_2O_2 for 24 h (i.e., oxidative stress tests). At the time of detection, the medium was removed, and 200 μL MTT reagent was added to the cells for 30 min. After incubation, the purple crystal sediment was dissolved in dimethyl sulfoxide and the absorbance was read at 540 nm using an ELISA reader. Absorbance was used to determine the cell number.

Flow cytometric analysis to determine the fluorescent intensity of reactive oxygen species (ROS)

To assess total intracellular and mitochondrial ROS, the cells were incubated in serum-free medium containing 10 μM H_2DCFDA, 5 μM MitoSOX, and 50 nM NAO in a 37 °C incubator for 20 min after rinsing the cells twice with phosphate-buffered saline (PBS). After rinsing twice with PBS to remove residual H_2DCFDA, the cells were incubated in serum-containing culture medium for an additional 30 min. Following trypsinization, the cells were suspended in PBS and analyzed using flow cytometry in the FL1 channel.

Induction of ICH by type IV collagenase proteolytic enzyme in rodent

The procedure and protocol of ICH were based on a recent report (Rana et al. 2019). The rats were anesthetized by inhalation of 2.0% isoflurane and placed on a warming pad at 37 °C, followed by securing the head and shaving the scalp hair. Under sterile conditions, a 1-cm long midline incision of the scalp was created to expose the perpendicular intersection point of the coronal and sagittal sutures (i.e., bregma). A Hamilton syringe (250 μL) was mounted onto the injection pump to stereotaxically guide the needle (26 gauge) over the bregma. The arms of the stereotactic manipulator were adjusted to move the needle 1.4 mm anterior and 3.2 mm lateral to the right. A small cranial burr hole was created using a 1 mm drill bit. Collagenase type IV (1.0 μL, 0.25 IU/μL) was injected into corpus/dorsal striatum (5 mm below the skull) through the 26 gauge Hamilton syringe at a rate of 0.2 μL/min. The syringe was slowly removed after injection, and sterile bone wax was used to quickly plug the hole. The skin on the head surface was closed using 4-0 prolene suture. Finally, the animals were recovered in a portable animal intensive care unit (ThermoCare®, Braintree Scientific, Pembroke, MA, USA) with food and water for 24 h.

Animal grouping and study period

Pathogen-free, adult male (i.e., 10–12 weeks old) SD rats (n = 50), weighing 325–350 g (Charles River Technology, BioLASCO, Taipei, Taiwan), were randomly categorized into group 1 [sham-operated control (SC)], group 2 (ICH + 20 μL culture medium), group 3 [ICH + Ex^{Mito} (350 μg) by intracranial injection at 3 h after ICH], group 4 [ICH + Ove-PrP^C-ADMSCs (6.0×10^5) cells by intracranial injection and 1.2×10^6 cells by intravenous injection, respectively], and group 5 [ICH + combined Ex^{Mito} (i.e., by intracranial administration) + Ove-PrP^C-ADMSCs]. The doses of mitochondrial ADMSCs were based on a previous report (Rana et al. 2019). Additionally, all animals were euthanized on day 28 after brain MRI. The brains were harvested from each group of animals for individual studies.

Procedure and protocol of brain MRI

The procedure and protocol for brain MRI studies were based on our previous report (Chen et al. 2014b). Brain MRI was performed 28 days after TBH induction. During MRI measurements, rats were anesthetized by 2.0% inhalational isoflurane with room air and placed in an MRI-compatible holder (Biospec 94/20, Bruker, Ettingen, Germany). The rectal temperature and respiration were monitored throughout the procedure to ensure that normal physiological conditions were maintained. MRI data were collected using a Varian 9.4 T animal scanner (Biospec 94/20, Bruker, Ettingen, Germany) with a rat surface array. The MRI protocol comprised 40 T2-weighted images. Forty continuous slice locations were imaged with a field of view of 30 × 30 mm, acquisition matrix dimensions of 256 × 256 mm, and slice thickness of 0.5 mm. The repetition time and echo time for each fast spin-echo volume were 4200 and 30 ms, respectively. ImageJ software (1.43i, NIH, Bethesda, MD, USA) was used to process data from the regions of interest. Planimetric measurements of T2 were performed to calculate the hemorrhagic volumes of the cortex. Collectively, the BHV was calculated by summing the total coronal sections and then dividing by the number of coronal sections to obtain the means of the IAs. Additionally, the height of the infarct zone was calculated by summing the thicknesses of each coronal section. Finally, the BHV was calculated as the mean IA × height.

Corner test for assessment of sensorimotor function

The sensorimotor function test (corner test) was conducted for each rat at baseline and on days 3, 7, 14, and 28 after acute ICH induction, as previously reported (Yip et al. 2020; Chen et al. 2014b; Rana et al. 2019). Briefly, rats in each group were allowed to walk through a tunnel and then into a 60° corner. The rats could turn either left or right to exit a corner. A technician blinded to the study design recorded the results. This test was repeated 10–15 times, with at least 30 s between each test. The technician recorded the number of right and left turns in 10 successful trials for each animal, and the results were statistically analyzed.

Identification of brain IA by TTC at day 14 after acute ICH procedure

The procedure and protocol were described in our previous report (Chen et al. 2014b). Briefly, brain axial sections of the rats were obtained from six animals in groups 2 and 3 (n = 6–7 for each group) as 2 mm slices. Each cross-section of the brain tissue was stained with 2% TTC (Alfa Aesar, Ward Hill, MA, USA) to analyze the brain IA. All brain sections were placed on a tray with a scaled vertical bar attached to a digital camera. Sections were photographed directly above from a fixed height. Images were analyzed using Image Tool 3 (IT3) image analysis software (UTHSCSA; Image Tool for Windows, Version 3.0; University of Texas, Health Science Center, San Antonio USA). The IA was observed as either whitish or pale yellowish. The infarcted region was confirmed by microscopic examination. The percentage of IA was obtained by dividing the IA by the total cross-sectional area of the brain.

IF staining

The procedure and protocol for IF staining was described in our previous reports (Yip et al. 2020; Chen et al. 2014b; Rana et al. 2019). Rehydrated paraffin sections were first treated with 3% H_2O_2 for 30 min and then incubated with the ImmunoBlock reagent (BioSB, Santa Barbara, CA, USA) for 30 min at room temperature. Sections were incubated with primary antibodies against CD68 (ab31630, 1:500, Abcam, Cambridge, UK), NeuN (MAB377, 1:100, Sigma, St. Louis, MO, USA), and r-H2AX (1:1000, Abcam). Sections incubated with irrelevant antibodies served as controls. Three brain tissue sections from each rat were analyzed. For quantification, three random high-power fields (400 × for IF studies) were analyzed in each section. The mean number of positively stained cells per high-power field for each animal was determined by summing all numbers divided by 9.

Western blot analysis

Western blot analysis was performed as described previously (Yip et al. 2020; Chen et al. 2014b; Rana et al. 2019). Briefly, equal amounts (50 μg) of protein extract were loaded and separated by sodium dodecyl sulfate–polyacrylamide gel electrophoresis using acrylamide gradients. After electrophoresis, the separated proteins were transferred onto polyvinylidene difluoride membranes (GE Healthcare, Little Chalfont, UK). Nonspecific sites were blocked by incubating the membrane in blocking buffer [5% nonfat dry milk in Tris-buffered saline containing 0.05% Tween 20)] overnight. The membranes were incubated with primary antibodies [Cyclin D1 (1:1000, Abcam), CyclinE1 (1:1000, Abcam), CDK2 (1:1000, Abcam), CDK4 (1:1000, Abcam), NOX1 (1:1000, Sigma), NOX4 (1:1000, Abcam), cytochrome C (1:10,000, BD Biosciences, Franklin Lakes, NJ, USA), p-DRP1 (1:1000, Cell Signaling Technology, Danvers, MA, USA), cyclophilin D (1:10,000, Abcam), PINK (1:10,000, Abcam), Beclin1 (1:1000, Cell Signaling Technology), Bax (1:1000, Abcam), cleaved caspase 3 (1:1000, Cell Signaling Technology), cleaved PARP (1:1000, Cell Signaling Technology), phosphorylated (p)-PI3K (1:1000, Cell Signaling Technology), PI3K (1:1000, Cell Signaling Technology), p-AKT (1:1000, Cell Signaling Technology), AKT (1:1000, Cell Signaling Technology), p-mTOR (1:1000, Abcam), mTOR (1:1000, Abcam), γ-H2AX (1:1000, Cell Signaling Technology), transforming growth factor beta (TGF-β) (1:1000, Abcam), p-Smad3 (1:1000, Cell Signaling Technology), COX-IV (1:10,000, Abcam), and actin (1:1000, Millipore, Billerica, MA, USA)] for 1 h at room temperature. Horseradish peroxidase-conjugated anti-rabbit immunoglobulin IgG (1:2000; Cell Signaling, Danvers, MA, USA) was used as the secondary antibody for 1-h incubation at room temperature. Washing was repeated eight times within 1 h. Immunoreactive bands were visualized using enhanced chemiluminescence (ECL; Amersham Biosciences, Amersham, UK) and exposed to Biomax L film (Kodak, Rochester, NY, USA). For quantification, ECL signals were digitized using Labwork software (UVP, Waltham, MA, USA).

Statistical analysis

Quantitative data are expressed as the mean ± standard deviation. Statistical analysis was performed using analysis of variance, followed by Bonferroni multiple-comparison post-hoc tests. SAS statistical software for Windows version 8.2 (SAS Institute, Cary, NC, USA) was used. Statistical significance was set at $P < 0.05$.

Supplementary Information The online version contains supplementary material available at https://doi.org/10.1007/s10735-025-10382-x.

Acknowledgements This study was supported by a program grant from Chang Gung Memorial Hospital, Chang Gung University (CMPRG8M0231) and National Science and Technology Council (NMRPG8M0281/MOST 111-2314-B-182A-147).

Author contributions Investigation: K. -C. L., J.-N. Y., P.-H. S., T. -C. Y., C. -R. H., T. -L. C. and Y. -T. W. Methodology: K. -C. L., T. -C. Y., C. -R. H. and P.-H. S. Funding acquisition: K. -C. L. Supervision: K. -C. L., K. -H. C. and H.-K. Y. Writing—review & editing, K. -C. L., J.-Y. C. and H.-K. Y. All authors read and approved the final manuscript" in the last statement.

Funding This study was supported by a program grant from Chang Gung Memorial Hospital, Chang Gung University (CMPRG8M0231) and National Science and Technology Council (NMRPG8M0281/

MOST 111–2314-B-182A-147).

Data availability No datasets were generated or analysed during the current study.

Declarations

Conflict of interest The authors declare no competing interests.

Ethical approval and consent for publication All animal experimental procedures were approved by the Institutional Animal Care and Use Committee at Kaohsiung Chang Gung Memorial Hospital (Affidavit of Approval of Animal Use Protocol No. 2021120204) and performed in accordance with the Guide for the Care and Use of Laboratory Animals, 8th edition (NIH publication No. 85–23, National Academy Press, Washington, DC, USA, revised 2011).

References

Albay CEQ, Leyson FGD, Cheng FC (2020) Dual versus mono antiplatelet therapy for acute non- cardio embolic ischemic stroke or transient ischemic attack, an efficacy and safety analysis—updated meta-analysis. BMC Neurol 20(1):224

An SJ, Kim TJ, Yoon BW (2017) Epidemiology, risk factors, and clinical features of intracerebral hemorrhage: an update. J Stroke 19(1):3–10

Bamford J, Sandercock P, Dennis M, Burn J, Warlow C (1991) Classification and natural history of clinically identifiable subtypes of cerebral infarction. Lancet 337(8756):1521–1526

Burchell SR, Tang J, Zhang JH (2017) Hematoma expansion following intracerebral hemorrhage: mechanisms targeting the coagulation cascade and platelet activation. Curr Drug Targets 18(12):1329–1344

Chen S, Zeng L, Hu Z (2014a) Progressing haemorrhagic stroke: categories, causes, mechanisms and managements. J Neurol 261(11):2061–2078

Chen HH, Lin KC, Wallace CG, Chen YT, Yang CC, Leu S, Chen YC, Sun CK, Tsai TH, Chen YL, Chung SY, Chang CL, Yip HK (2014b) Additional benefit of combined therapy with melatonin and apoptotic adipose-derived mesenchymal stem cell against sepsis-induced kidney injury. J Pineal Res 57(1):16–32

Chen KH, Chen CH, Wallace CG, Yuen CM, Kao GS, Chen YL, Shao PL, Chen YL, Chai HT, Lin KC, Liu CF, Chang HW, Lee MS, Yip HK (2016a) Intravenous administration of xenogenic adipose-derived mesenchymal stem cells (ADMSC) and ADMSC-derived exosomes markedly reduced brain infarct volume and preserved neurological function in rat after acute ischemic stroke. Oncotarget 7(46):74537–74556

Chen HH, Chen YT, Yang CC, Chen KH, Sung PH, Chiang HJ, Chen CH, Chua S, Chung SY, Chen YL, Huang TH, Kao GS, Chen SY, Lee MS, Yip HK (2016b) Melatonin pretreatment enhances the therapeutic effects of exogenous mitochondria against hepatic ischemia-reperfusion injury in rats through suppression of mitochondrial permeability transition. J Pineal Res 61(1):52–68

Chen YT, Yang CC, Chiang JY, Sung PH, Shao PL, Huang CR, Lee MS, Yip HK (2023) Prion protein overexpression in adipose-derived mesenchymal stem cells (ADMSCs) effectively protected rodent kidney against ischemia-reperfusion injury via enhancing ATP/Mitochondrial biogenesis-ROLE of ADMSC rejuvenation and proliferation. Cell Transpl 32:9636897231211068

Collaborators GBDN (2019) Global, regional, and national burden of neurological disorders, 1990–2016: a systematic analysis for the Global Burden of Disease Study 2016. Lancet Neurol 18(5):459–480

Duan X, Wen Z, Shen H, Shen M, Chen G (2016) Intracerebral hemorrhage oxidative stress, and antioxidant therapy. Oxid Med Cell Longev 2016:1203285

Gaiqing W (2014) The Pathogenesis of Edema and Secondary Insults after ICH. In: Vikas C (ed) Intracerebral Hemorrhage. IntechOpen, Rijeka, p 3

Gauberti M, Martinez de Lizarrondo S, Vivien D (2021) Thrombolytic strategies for ischemic stroke in the thrombectomy era. J Thromb Haemost 19(7):1618–1628

Haupenthal D, Kuramatsu JB, Volbers B, Sembill JA, Mrochen A, Balk S, Hoelter P, Lucking H, Engelhorn T, Dorfler A, Schwab S, Huttner HB, Sprugel MI (2021) Disability-adjusted life-years associated with intracerebral hemorrhage and secondary injury. JAMA Netw Open 4(7):e2115859

Hemphill JC 3rd, Greenberg SM, Anderson CS, Becker K, Bendok BR, Cushman M, Fung GL, Goldstein JN, Macdonald RL, Mitchell PH, Scott PA, Selim MH, Woo D (2015) Council on clinical, guidelines for the management of spontaneous intracerebral hemorrhage: a guideline for healthcare professionals from the American heart association/American stroke association. Stroke 46(7):2032–60

Henderson SJ, Weitz JI, Kim PY (2018) Fibrinolysis: strategies to enhance the treatment of acute ischemic stroke. J Thromb Haemost 16(10):1932–1940

Hostettler IC, Seiffge DJ, Werring DJ (2019) Intracerebral hemorrhage: an update on diagnosis and treatment. Expert Rev Neurother 19(7):679–694

Hu X, Tao C, Gan Q, Zheng J, Li H, You C (2016) Oxidative stress in intracerebral hemorrhage: sources mechanisms, and therapeutic targets. Oxid Med Cell Longev 2016:3215391

Kim J, Thayabaranathan T, Donnan GA, Howard G, Howard VJ, Rothwell PM, Feigin V, Norrving B, Owolabi M, Pandian J, Liu L, Cadilhac DA, Thrift AG (2020) Global Stroke Statistics 2019. Int J Stroke 15(8):819–838

Ko SF, Chen KH, Wallace CG, Yang CC, Sung PH, Shao PL, Li YC, Chen YT, Yip HK (2020) Protective effect of combined therapy with hyperbaric oxygen and autologous adipose-derived mesenchymal stem cells on renal function in rodent after acute ischemia-reperfusion injury. Am J Transl Res 12(7):3272–3287

Lee FY, Shao PL, Wallace CG, Chua S, Sung PH, Ko SF, Chai HT, Chung SY, Chen KH, Lu HI, Chen YL, Huang TH, Sheu JJ, Yip HK (2018) Combined therapy with SS31 and mitochondria mitigates myocardial ischemia-reperfusion injury in rats. Int J Mol Sci 19(9):2782

Lin KC, Yip HK, Shao PL, Wu SC, Chen KH, Chen YT, Yang CC, Sun CK, Kao GS, Chen SY, Chai HT, Chang CL, Chen CH, Lee MS (2016) Combination of adipose-derived mesenchymal stem cells (ADMSC) and ADMSC-derived exosomes for protecting

kidney from acute ischemia-reperfusion injury. Int J Cardiol 216:173–185
Lin KC, Wallace CG, Yin TC, Sung PH, Chen KH, Lu HI, Chai HT, Chen CH, Chen YL, Li YC, Shao PL, Lee MS, Sheu JJ, Yip HK (2018) Shock wave therapy enhances mitochondrial delivery into target cells and protects against acute respiratory distress syndrome. Mediators Inflamm 2018:5425346
Lin KC, Yeh JN, Chen YL, Chiang JY, Sung PH, Lee FY, Guo J, Yip HK (2020) Xenogeneic and allogeneic mesenchymal stem cells effectively protect the lung against ischemia-reperfusion injury through downregulating the inflammatory. Oxid Stress Autophagic Signal Pathw Rat Cell Transpl 29:963689720954140
Minnerup J, Wersching H, Teuber A, Wellmann J, Eyding J, Weber R, Reimann G, Weber W, Krause LU, Kurth T, Berger K, Investigators R (2016) Outcome after thrombectomy and intravenous thrombolysis in patients with acute ischemic stroke: a prospective observational study. Stroke 47(6):1584–1592
Mittal MK, LacKamp A (2016) Intracerebral hemorrhage: perihemorrhagic edema and secondary hematoma expansion: from bench work to ongoing controversies. Front Neurol 7:210
Mittal MK, Lele A (2011) Predictors of poor outcome at hospital discharge following a spontaneous intracerebral hemorrhage. Int J Neurosci 121(5):267–270
Montano A, Hanley DF, Hemphill JC 3rd (2021) Hemorrhagic stroke. Handb Clin Neurol 176:229–248
O'Carroll CB, Brown BL, Freeman WD (2021) Intracerebral hemorrhage: a common yet disproportionately deadly stroke subtype. Mayo Clin Proc 96(6):1639–1654
Ojaghihaghighi S, Vahdati SS, Mikaeilpour A, Ramouz A (2017) Comparison of neurological clinical manifestation in patients with hemorrhagic and ischemic stroke. World J Emerg Med 8(1):34–38
Padovani A, Pilotto A (2020) Looking at the burden of neurological disorders in Europe. Lancet Public Health 5(10):e523
Pinzon RT, Wijaya VO (2020) Complications as poor prognostic factors in patients with hemorrhagic stroke: a hospital-based stroke registry. Int J Neurol Neurother 19(1):12–20
Powers WJ, Rabinstein AA, Ackerson T, Adeoye OM, Bambakidis NC, Becker K, Biller J, Brown M, Demaerschalk BM, Hoh B, Jauch EC, Kidwell CS, Leslie-Mazwi TM, Ovbiagele B, Scott PA, Sheth KN, Southerland AM, Summers DV, Tirschwell DL, C. (2018) American heart association stroke, 2018 guidelines for the early management of patients with acute ischemic stroke: a guideline for healthcare professionals from the American heart association/American stroke association. Stroke 49(3):e46–e110
Powers WJ, Rabinstein AA, Ackerson T, Adeoye OM, Bambakidis NC, Becker K, Biller J, Brown M, Demaerschalk BM, Hoh B, Jauch EC, Kidwell CS, Leslie-Mazwi TM, Ovbiagele B, Scott PA, Sheth KN, Southerland AM, Summers DV, Tirschwell DL (2019) Guidelines for the early management of patients with acute ischemic stroke: 2019 update to the 2018 guidelines for the early management of acute ischemic stroke: a guideline for healthcare professionals from the American heart association/American stroke association. Stroke 50(12):e344–e418
Rana NK, Singh P, Koch B (2019) CoCl(2) simulated hypoxia induce cell proliferation and alter the expression pattern of hypoxia associated genes involved in angiogenesis and apoptosis. Biol Res 52(1):12
Rangel-Castilla L, Snyder KV, Siddiqui AH, Levy EI, Hopkins NL (2016) Endovascular intracranial treatment of acute ischemic strokes. J Cardiovasc Surg (Torino) 57(1):36–47
Reyes R, Viswanathan M, Aiyagari V (2019) An update on neurocritical care for intracerebral hemorrhage. Expert Rev Neurother 19(6):557–578
Rodrigues FB, Neves JB, Caldeira D, Ferro JM, Ferreira JJ, Costa J (2016) Endovascular treatment versus medical care alone for ischaemic stroke: systematic review and meta-analysis. BMJ 353:i1754
Roucou X, Giannopoulos PN, Zhang Y, Jodoin J, Goodyer CG, LeBlanc A (2005) Cellular prion protein inhibits proapoptotic Bax conformational change in human neurons and in breast carcinoma MCF-7 cells. Cell Death Differ 12(7):783–795
Shao Z, Tu S, Shao A (2019) Pathophysiological mechanisms and potential therapeutic targets in intracerebral hemorrhage. Front Pharmacol 10:1079
Smith WS (2019) Endovascular stroke therapy. Neurotherapeutics 16(2):360–368
StatPearls Publishing (2023) Copyright © 2023, StatPearls Publishing LLC., Treasure Island (FL) with ineligible companies. Disclosure: Joe M Das declares no relevant financial relationships with ineligible companies. Disclosure: Parth Mehta declares no relevant financial relationships with ineligible companies.
Testai FD, Aiyagari V (2008) Acute hemorrhagic stroke pathophysiology and medical interventions: blood pressure control, management of anticoagulant-associated brain hemorrhage and general management principles. Neurol Clin 26(4):963–85
Unnithan AKA, Mehta P (2023) Hemorrhagic Stroke, StatPearls, StatPearls Publishing
Weissmann C (2004) The state of the prion. Nat Rev Microbiol 2(11):861–871
Wu F, Liu Z, Li G, Zhou L, Huang K, Wu Z, Zhan R, Shen J (2021) Inflammation and oxidative stress: potential targets for improving prognosis after subarachnoid hemorrhage. Front Cell Neurosci 15:739506
Xiong Y, Bath PM (2020) Antiplatelet therapy for transient ischemic attack and minor stroke. Stroke 51(11):3472–3474
Yin TC, Li YC, Sung PH, Chiang JY, Shao PL, Yip HK, Lee MS (2023) Adipose-derived mesenchymal stem cells overexpressing prion improve outcomes via the NLRP3 inflammasome/DAMP signalling after spinal cord injury in rat. J Cell Mol Med 27(4):482–495
Yip HK, Chang YC, Wallace CG, Chang LT, Tsai TH, Chen YL, Chang HW, Leu S, Zhen YY, Tsai CY, Yeh KH, Sun CK, Yen CH (2013) Melatonin treatment improves adipose-derived mesenchymal stem cell therapy for acute lung ischemia-reperfusion injury. J Pineal Res 54(2):207–221
Yip HK, Shao PL, Wallace CG, Sheu JJ, Sung PH, Lee MS (2020) Early intramyocardial implantation of exogenous mitochondria effectively preserved left ventricular function in doxorubicin-induced dilated cardiomyopathy rat. Am J Transl Res 12(8):4612–4627
Yip HK, Dubey NK, Lin KC, Sung PH, Chiang JY, Chu YC, Huang CR, Chen YL, Deng YH, Cheng HC, Deng WP (2021a) Melatonin rescues cerebral ischemic events through upregulated tunneling nanotube-mediated mitochondrial transfer and downregulated mitochondrial oxidative stress in rat brain. Biomed Pharmacother 139:111593
Yip HK, Lin KC, Sung PH, Chiang JY, Yin TC, Wu RW, Chen KH (2021b) Umbilical cord-derived MSC and hyperbaric oxygen therapy effectively protected the brain in rat after acute intracerebral haemorrhage. J Cell Mol Med 25(12):5640–5654
Zheng H, Chen C, Zhang J, Hu Z (2016) Mechanism and therapy of brain edema after intracerebral hemorrhage. Cerebrovasc Dis 42(3–4):155–169
Zomosa-Signoret V, Arnaud JD, Fontes P, Alvarez-Martinez MT, Liautard JP (2008) Physiological role of the cellular prion protein. Vet Res 39(4):9

Authors and Affiliations

Kun-Chen Lin[1] · Jui-Ning Yeh[2,3] · Pei-Hsun Sung[4,5,6] · Tsung-Cheng Yin[7,8] · John Y. Chiang[9,10] · Chi-Ruei Huang[4,5] · Yi-Ling Chen[4,6] · Yi-Ting Wang[4,6] · Kuan-Hung Chen[1] · Hon-Kan Yip[4,5,6,11,12]

✉ Kuan-Hung Chen
amigofx35@gmail.com

✉ Hon-Kan Yip
han.gung@msa.hinet.net

1 Department of Anesthesiology, Kaohsiung Chang Gung Memorial Hospital and Chang Gung University College of Medicine, Niaosung Dist, No. 123, Dapi Rd., Kaohsiung 833401, Taiwan, ROC

2 Institute of Nephrology and Blood Purification, the First Affiliated Hospital of Jinan University, Jinan University, Guangzhou 510632, China

3 Department of Cardiology, The First Affiliated Hospital, Jinan University, Guangzhou 510632, China

4 Division of Cardiology, Department of Internal Medicine, Kaohsiung Chang Gung Memorial Hospital and Chang Gung University College of Medicine, Niaosung Dist, No. 123, Dapi Rd., Kaohsiung 833401, Taiwan, ROC

5 Center for Shockwave Medicine and Tissue Engineering, Kaohsiung Chang Gung Memorial Hospital, Kaohsiung 833401, Taiwan, ROC

6 Institute for Translational Research in Biomedicine, Kaohsiung Chang Gung Memorial Hospital, Kaohsiung 833401, Taiwan, ROC

7 Department of Orthopedics, Kaohsiung Chang Gung Memorial Hospital and Chang Gung University College of Medicine, Kaohsiung 833401, Taiwan, ROC

8 Center for General Education, Cheng Shiu University, Kaohsiung, Taiwan, ROC

9 Department of Computer Science and Engineering, National Sun Yat-Sen University, Kaohsiung 804201, Taiwan, ROC

10 Department of Healthcare Administration and Medical Informatics, Kaohsiung Medical University, Kaohsiung 807378, Taiwan, ROC

11 Department of Medical Research, China Medical University Hospital, China Medical University, Taichung 404333, Taiwan, ROC

12 School of Medicine, College of Medicine, Chang Gung University, Taoyuan 333323, Taiwan, ROC